BIOCHEMISTRY
including biophysical chemistry & molecular biology

Article

pubs.acs.org/biochemistry

Unraveling the Phosphocholination Mechanism of the *Legionella pneumophila* Enzyme AnkX

Konstantin Gavriljuk,[†,∥] Jonas Schartner,[†] Hans Seidel,[†,∥] Clarissa Dickhut,[‡] Rene P. Zahedi,[‡] Christian Hedberg,[§] Carsten Kötting,[*,†] and Klaus Gerwert[*,†]

[†]Department of Biophysics, Ruhr-Universität Bochum, Universitätsstrasse 150, 44801 Bochum, Germany

[‡]Leibniz-Institut für Analytische Wissenschaften-ISAS-e.V., Otto-Hahn-Strasse 6b, 44227 Dortmund, Germany

[§]Department of Chemistry and Umeå Center for Microbial Research, Umeå University, SE-90187 Umeå, Sweden

Supporting Information

ABSTRACT: The intracellular pathogen *Legionella pneumophila* infects lung macrophages and injects numerous effector proteins into the host cell to establish a vacuole for proliferation. The necessary interference with vesicular trafficking of the host is achieved by modulation of the function of Rab GTPases. The effector protein AnkX chemically modifies Rab1b and Rab35 by covalent phosphocholination of serine or threonine residues using CDP-choline as a donor. So far, the phosphoryl transfer mechanism and the relevance of observed autophosphocholination of AnkX remained disputable. We designed tailored caged compounds to make this type of enzymatic reaction accessible for time-resolved Fourier transform infrared difference spectroscopy. By combining spectroscopic and biochemical methods, we determined that full length AnkX is autophosphocholinated at Ser521, Thr620, and Thr943. However, autophosphocholination loses specificity for these sites in shortened constructs and does not appear to be relevant for the catalysis of the phosphoryl transfer. In contrast, transient phosphocholination of His229 in the conserved catalytic motif might exist as a short-lived reaction intermediate. Upon substrate binding, His229 is deprotonated and locked in this state, being rendered capable of a nucleophilic attack on the pyrophosphate moiety of the substrate. The proton that originated from His229 is transferred to a nearby carboxylic acid residue. Thus, our combined findings support a ping-pong mechanism involving phosphocholination of His229 and subsequent transfer of phosphocholine to the Rab GTPase. Our approach can be extended to the investigation of further nucleotidyl transfer reactions, which are currently of reemerging interest in regulatory pathways of host−pathogen interactions.

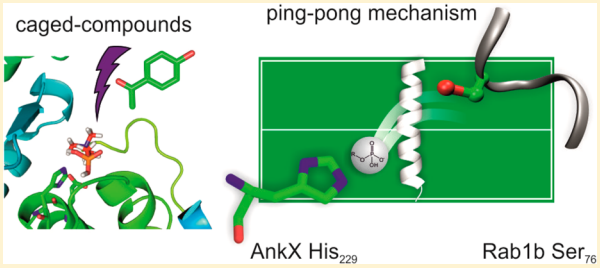

The bacterium *Legionella pneumophila* hijacks human lung macrophages by manipulation of cellular processes such as vesicle transport.[1−5] Via the use of a type IV secretion system (TFSS), a large number of effector proteins are inserted into the host cell creating a Legionella-containing vacuole (LCV). The pathogen proliferates in the LCV, finally leading to cell lysis.[3,5] Redirection of vesicular transport requires interference with the function of small GTPases of the Rab and Arf families, major regulators of vesicular trafficking.[6] The ankyrin repeat-containing protein AnkX is one of the *Legionella* effectors, functioning as a phosphocholine transferase that manipulates Rab proteins in the host cell.[7]

Covalent modification of GTPases by bacterial pathogens is a common principle involving FIC domain (filamentation induced by cAMP)-containing proteins in most cases.[8] The FIC domain of AnkX catalyzes the transfer of a phosphocholine moiety, but FIC domains generally can introduce a variety of modifications, such as adenylylation, uridylylation, guanylylation, and phosphorylation.[9,10] Notably, the adenylylase domain of DrrA, also a Legionella effector that modifies Rab1b, is not a FIC domain despite performing an analogous reaction.[11,12] Well-studied examples of FIC domain proteins are, for instance, VopS and IbpA, which catalyze adenylylation of Rho GTPases disrupting the actin cytoskeleton of the host cell.[13,14] In all cases, a phosphorus anhydride is cleaved by the conserved FIC motif [HXFX(D/E)(A/G)N(G/K)R] and a phosphodiester linkage to an OH group of the modified protein is formed.

To establish the LCV, *L. pneumophila* specifically targets the Rab GTPases Rab1b and Rab35, which regulate endoplasmatic reticulum to Golgi trafficking and cargo recycling at endosomes, respectively.[7,15,16] Rab GTPases are molecular switches cycling between the active GTP-bound "on" and the inactive GDP-bound "off" states. Interaction with various effectors via the so-called switch regions takes place in only the GTP-bound form. Nucleotide exchange is catalyzed by GEFs (guanine nucleotide exchange factors), and hydrolysis of GTP is catalyzed by GAPs (GTPase-activating proteins), thereby inactivating the switch.[17] Membrane tethering of Rab GTPases is mediated by C-terminal geranylgeranylation,[18,19] and membrane extraction is

Received: May 24, 2016
Revised: July 6, 2016
Published: July 12, 2016

ACS Publications © 2016 American Chemical Society

DOI: 10.1021/acs.biochem.6b00524
Biochemistry 2016, 55, 4375−4385

performed by GDI (GDP dissociation inhibitor) to recycle the GDP-bound Rab as a soluble cytosolic complex.[20] Rab35 is phosphocholinated by AnkX at Thr76 in the switch II region and Rab1b at the corresponding residue Ser76 with a slight preference for the GDP state of the GTPase.[7,21] For additional regulation, the pathogen provides the dephosphocholinase Lem3.[21] Most importantly, phosphocholination prevents the interaction with GDI and thus traps Rab at the membrane preferably in the GDP state.[21,22] Phosphocholination impairs the interaction with GEFs but does not greatly affect the interaction with GAPs or the *Legionella* supereffector LidA, although the implications of the latter are not clear yet.[21] Rab35 has also been shown to be involved in cancer development by mislocalization of PDGFR (platelet-derived growth factor receptor) to endosomes by Rab35Q67L, which is less sensitive to inactivation by GAPs (GTPase-activating proteins), without altering vesicle morphology.[23] Therefore, interfering with Rab35 function by *Legionella* might not directly impact vesicle transport but rather involve relocalization of yet unidentified factors in pathways that influence early endosome maturation and thus promote LCV formation.

Recently, the reversible phosphocholination catalyzed by AnkX/Lem3 has been harnessed in a universal fluorescence labeling/delabeling approach, which requires only the introduction of a Rab1b-derived peptide into the target protein.[24] This novel application is made possible by the fact that AnkX accepts not only CDP-choline as the cofactor but also CDP and its derivatives with large substituents at the β-phosphate. Recently, progress has been made in understanding the catalytic mechanism of AnkX by resolving the crystal structure of the AnkX FIC domain, which explains the ability of FIC domains to utilize different substrates such as ATP, UDP-glucose, or CDP-choline.[25] The nucleotide can be bound in different orientations allowing the transfer of either the sugar-containing moiety or the terminal phosphoryl group. In either case, a conserved histidine residue in the FIC motif is indispensable for breakage of the phosphorus anhydride and transfer of phosphocholine to the hydroxyl group of Rab35 or Rab1b. Previously, a ping-pong mechanism for this enzymatic reaction was suggested by steady-state kinetic analysis,[21] but a concerted transfer was proposed on the basis of the crystal structure.[25] The ping-pong mechanism would involve transient transfer of phosphocholine to His229 of AnkX prior to phosphocholination of Ser76/Thr76 of the substrate. The concerted mechanism suggests an in-line nucleophilic attack of Ser76/Thr76 on the β-phosphate of CDP-choline. An important consideration for the reaction mechanism is the observation of autophosphocholination of AnkX in both studies. However, different sites for autophosphocholination have been proposed leading to contradictory implications for the activity of AnkX and possible transient phosphocholination of the catalytic histidine residue.

Fourier transform infrared (FTIR) difference spectroscopy (static or time-resolved) fully resolves protein mechanisms in atomic detail in real time without any label.[26] Infrared spectra possess a very high information content because every single chemical group makes a distinct contribution to the overall spectrum. The functional residues are selectively resolved from the background absorbance by computing the difference between the ground state and reaction intermediates.[27] Pioneering work applied this technique to light-inducible chromo-protein reactions, such as in photosystems[28,29] or rhodopsins.[30,31] Over the past decades, noncyclic protein reactions were addressed by us and others employing caged compounds.[32,33]

Still, the studied targets were mainly limited to GTPases and ATPases. We seek to establish time-resolved FTIR spectroscopy as a general tool that can be applied to diverse biological questions. Thus, a crucial prerequisite is the design of caged compounds tailored to the targeted enzyme class. Recently, we already expanded this approach to adenylyltransferases and unraveled the molecular mechanism of the *Legionella* effector DrrA.[11] To resolve the unclear details of AnkX-catalyzed phosphocholine transfer as outlined above, we designed five novel photocleavable CDP derivatives, including isotopically labeled compounds. Our combined biochemical and spectroscopic data provide insights into the molecular mechanism of the phosphocholine transfer reaction catalyzed by AnkX. With these data, we propose a ping-pong mechanism based on the catalytic His229 as a key residue for the enzymatic modification of Rab GTPases.

EXPERIMENTAL PROCEDURES

All chemicals and organic solvents were purchased from Sigma-Aldrich. Chemical structures of the synthesized compounds are presented in Supplementary Figure 1.

Synthesis of 1-(2-Nitro)phenylethyl-cytidinediphosphate Choline (npe-CDP choline). The synthesis was conducted as described previously.[11,34] CDP-choline (350 mg, 0.72 mmol) was dissolved in 3 mL of water, and an excess of 1-(2-nitrophenyl)diazoethane was added every 12 h (1 g total). The pH was adjusted to 3−4 and kept constant by adding HCl if necessary. The reaction mixture was stirred vigorously in the dark and controlled by analytical high-performance liquid chromatography (HPLC). After 5 days, the chloroform phase was removed and the water phase was washed three times (10 mL of chloroform). Subsequently, npe-CDP-choline was purified over an anion exchange column (diethylaminoethyl resin, DEAE) with a gradient (0 to 250 mM) of triethylaminobutyl buffer (TEAB, pH 8). The product fractions were pooled, concentrated, and analyzed by HPLC and fast atom bombardment mass spectrometry (FAB-MS): M = 638.1 g mol^{-1} $[M + H]^+$, M = 660.1 g mol^{-1} $[M + Na]^+$. The yield was 100 mg (22%).

Synthesis of 1-(2-Nitro)phenylethyl-cytidinediphosphate (npe-CDP). Briefly, 100 mg (0.25 mmol) of npe-CDP was dissolved in 5 mL of water, and an excess of 1-(2-nitrophenyl)diazoethane was added. The reaction was finished after 48 h. The purification was conducted as described for npe-CDP-choline with a 0 to 240 mM TEAB gradient. FAB-MS: M = 553.0 g mol^{-1} $[M + H]^+$, M = 575.0 g mol^{-1} $[M + Na]^+$. The yield was 52 mg (38%).

Synthesis of β-$^{18}O_4$-1-(2-Nitro)phenylethyl-cytidinediphosphate (β-$^{18}O_4$-npe-CDP). In the first step, ^{18}O-labeled P_i was synthesized (Supplementary Figure 2).[35] Phosphorus pentachloride (2.5 g) was cooled in a round-bottom flask under an argon atmosphere. Very slowly, 1 g of $H_2{}^{18}O$ was added and the mixture stirred for 20 min. After the addition of 900 μL of tributylamine, the mixture was stirred for a further 10 min. The obtained product was concentrated in vacuum and subsequently co-evaporated with dry pyridine (2 × 900 μL). The white product was dried under reduced pressure and characterized via FAB-MS: M (tributylamine phosphate) = 477.4 g mol^{-1} $[M + H]^+$. In the second step, 200 mg (0.62 mmol) of CMP was dissolved in 1 mL of water and purified over a Dowex 50W resin to remove the sodium ions.[36] The

DOI: 10.1021/acs.biochem.6b00524
Biochemistry 2016, 55, 4375−4385

activation of CMP was achieved on the basis of the work of Park and Givens.[36] To the activated CMP was added 1.2 g (2.52 mM) of the ^{18}O-labeled phosphate in 15 mL of DMF. The mixture was stirred under an argon atmosphere for 48 h. The reaction was monitored by analytical HPLC. The purification was conducted as described for npe-CDP-choline with a 0 to 170 mM TEAB gradient. FAB-MS: M = 433.9 g mol^{-1} [M + Na]$^+$. The yield was 40 mg (16%). The second synthesis step was repeated to obtain sufficient amounts of the product. Finally, 55 mg (0.13 mmol) of $^{18}O_4$-CDP was dissolved in 6 mL of water, and 4 mL of 1-(2-nitrophenyl)-diazoethane in chloroform (600 mg) was added. The pH was adjusted to 3−4, and the mixture was stirred in the dark for 24 h. The progress of the reaction was controlled via analytical HPLC. The purification was done as described above with a 0 to 240 mM TEAB gradient. ESI-MS: M = 560.5 g mol^{-1} [M + H]$^+$. The yield was 19 mg (26%).

Synthesis of 4-Hydroxyphenacyl-cytidinediphosphate (php-CDP). The synthesis was conducted as described by Park and Givens.[36] Briefly, 50 mg (0.15 mmol) of CMP was purified over a Dowex 50w resin, activated with carbonyldiimidazole, and mixed with 105 mg (0.46 mmol) of php-phosphate in dry DMF for 80 h in the dark. The progress of the reaction was monitored via analytical HPLC. The purification was conducted as described for the npe compounds with a 0 to 260 mM TEAB gradient. ESI-MS: M = 536.2 g mol^{-1} [M + H]$^+$. The yield was 20 mg (25%).

Synthesis of α-$^{18}O_2$-4-Hydroxyphenacyl-cytidinediphosphate (α-$^{18}O_2$-php-CDP). In the first synthesis step, ^{18}O-CMP was generated as described by Goody (Supplementary Figure 3).[37] Briefly, 178 mg (0.8 mmol) of pentachlorophosphane was reacted with $H_2{}^{18}O$ (68 μL, 3.8 mmol), yielding ^{18}O-labeled phosphorous acid, which was further reacted with 200 mg of cytidine (0.8 mmol). The crude product was purified with a 0 to 180 mM TEAB gradient on a DEAE column. The yield was 68 mg (25%). The product ^{18}O-CMP was prepared as described for php-CDP to covalently attach a parahydroxyphenacyl group.[36] For purification, a TEAB gradient (0 to 220 mM) was employed that yielded 7 mg of α-$^{18}O_2$-php-CDP (6%). ESI-MS: M = 561.89 g mol^{-1} [M + Na]$^+$.

Protein Expression and Purification. Rab1b$_{3-174}$ and diverse AnkX constructs were expressed in *Escherichia coli* BL21 DE3 RIL and purified via Ni-NTA and gel filtration chromatography as described elsewhere.[21,38] The final gel filtration buffer consisted of 50 mM Hepes (pH 7.5), 200 mM NaCl, and 2 mM DTT (with 2 mM $MgCl_2$ and 20 μM GDP for Rab1b). For isotopic labeling of AnkX$_{1-484}$, bacteria were grown in 1.5 L of synthetic M9 medium[38] with histidine replaced by the labeled variant. For FTIR measurements, AnkX was concentrated to 60−85 mg/mL to minimize salt concentrations in the final samples. Usually, one would achieve this by exchanging the buffer with a low-ionic strength variant, but AnkX is very sensitive to salt concentration.

Fluorescence Measurements. The phosphocholination of Rab1b$_{3-174}$ catalyzed by AnkX was monitored by tryptophan fluorescence.[21] In a cuvette (1 mL), 10 μM Rab1b and 400 μM CDP-choline were stirred in a buffer containing 50 mM Hepes, 200 mM NaCl, 2 mM $MgCl_2$, 2 mM DTT, and 20 μM GDP. The temperature was adjusted to 25 °C, and the desired AnkX construct (200 nM) was added to start the reaction. The sample was excited at 297 nm, and the emission was detected at 340 nm, recording data points every 2 s. All errors are given as the standard deviation (SD).

HPLC/MS Analysis. For the investigation of substrate autohydrolysis by AnkX, 2 μM AnkX was incubated with 1 mM substrate at 25 °C in 50 mM Hepes, 200 mM NaCl, 2 mM $MgCl_2$, and 2 mM DTT. Samples were taken every 20 min and analyzed by reverse phase HPLC (C18 Prontosil, Bischoff GmbH) in 50 mM KP_i (pH 6.6), 5 mM TBAB, and 14% acetonitrile. Calibration of the analytical column allowed us to determine the amount and/or concentration of hydrolyzed substrate. For MS, the sample composition was similar, except that 50 μM AnkX was used and the samples were incubated for 1 h at 25 °C prior to analysis by LC−ESI-MS. For shotgun LC−MS analysis, approximately 10 pmol of AnkX in 50 ammonium bicarbonate was first reduced with 10 mM DTT for 30 min at 56 °C, followed by alkylation of free sulfhydryl groups with 30 mM iodoacetamide at room temperature in the dark. Trypsin (Promega, sequencing grade) was added (1:30), and the sample was digested for 8 h at 37 °C. Next, 200 fmol of proteolytic digest was analyzed by shotgun nano LC−MS using a U3000 RSLC nano-LC instrument coupled to an Orbitrap Velos ETD mass spectrometer (both from Thermo Scientific). Peptides were preconcentrated on a 75 μm × 2 cm C18 trapping column using 0.1% trifluoroacetic acid at a flow rate of 20 μL/min, followed by separation on a 75 μm × 50 cm C18 main column (both Pepmap Viper, Thermo Scientific) with a 60 min LC gradient ranging from 2 to 38% acetonitrile in 0.1% formic acid, at a flow rate of 250 nL/min. MS survey scans were acquired from m/z 300 to 2000 in the Orbitrap at a resolution of 60000 using the polysiloxane m/z 445.1200 as the lock mass. The five most intense ions were selected for data-dependent electron transfer dissociation (ETD) with an isolation width of m/z 2.0 and an activation time of 200 ms. Raw files were processed with Proteome Discoverer 1.4 (Thermo Scientific) using Mascot 2.4 (Matrix Science) as a search engine, ptmRS, an advanced version of the widely used phosphoRS algorithm,[39] for determining localization probabilities for identified phosphocholination sites, and the target/decoy PSM Validator. MS/MS spectra were searched against a Uniprot fasta database (July 2012) with taxonomy set to Proteobacteria (196376 target sequences) and the following settings: (i) trypsin as the enzyme with a maximum of two allowed missed cleavages, (ii) carbamidomethylation of Cys (+57.0214 Da) as fixed and phosphocholination of His, Ser, and Thr (+165.0554 Da) as well as oxidation of Met (+15.9949 Da) as variable modifications, (iii) MS and MS/MS tolerances of 10 ppm and 0.5 Da, respectively, and (iv) the instrument set to ETD trap. Obtained peptide-spectrum matches were filtered for a false discovery rate of <1% (high degree of confidence). Only three phosphocholinated peptides passed the 1% FDR filter, all of them belonging to AnkX. All three corresponding phosphocholination sites, namely, Ser521, Thr620, and Thr943, were highly confident and had ptmRS probabilities of ≥99% as well as Mascot delta scores of >13.

FTIR Measurements and Data Analysis. For FTIR measurements, Rab1b$_{3-174}$·GDP was subjected to buffer exchange with 1 mM Hepes (pH 7.5), 2 mM NaCl, 0.05 mM $MgCl_2$, and 0.05 mM DTT via a NAP-5 column (GE Life Sciences). AnkX proteins were concentrated as described above. Incubation of AnkX with caged substrates and subsequent removal of excess compound by desalting would yield apoprotein only, showing that AnkX does not bind the

DOI: 10.1021/acs.biochem.6b00524
Biochemistry 2016, 55, 4375−4385

caged substrates. Therefore, an equivalent amount of caged substrate needed to be added to the FTIR sample directly.

The FTIR sample was prepared between two BaF_2 windows as described previously[40] except that no mylar spacer was used because BaF_2 windows with a 10 μm deep cavity (S-Optics) allowed us to prepare vacuum stable cuvettes. The final sample composition was 4 mM Rab1b (where applicable), 4.8 mM AnkX, 20 mM $MgCl_2$, 20 mM DTT, 200 mM Hepes (pH 7.5), 600−800 mM NaCl, and 4 mM caged compound. Exceptional care needs to be taken during gentle drying of the sample with a nitrogen stream not to damage the proteins. Therefore, AnkX was usually the last component added and concentrated very quickly before addition of the final volume (0.6 μL) of 0.2% ethylene glycol or 18% ethylene glycol in water for the low-temperature measurements. Experiments for the analysis of Rab1b modification by AnkX were performed at 288 K, whereas the precatalytic conformational change of AnkX was measured at 257 K. At least 10 individual measurements were averaged to obtain the difference spectra with a good signal-to-noise ratio. Photolysis of the caged compounds was performed using an LPX 240 XeCl-excimer laser (308 nm; Lambda Physics/Coherent Laser Systems) by 40 flashes within 80 ms for npe-caged compounds, and 12 flashes within 24 ms for php-caged compounds. This leads to decaging of more than 90% of the respective compound. Unreacted caged compounds do not contribute to our difference spectra. A modified Bruker IFS 66v/s or Vertex 80v spectrometer in fast-scan mode was used for the measurement.[41] The data were analyzed between 1800 and 900 cm^{-1} with a global fit method.[42] In this analysis, the absorbance changes (ΔA) are analyzed with a sum of exponentials with apparent rate constants k_l and amplitudes a_l.

$$\Delta A(\tilde{\nu}, t) = \sum_{l=1}^{n_r} a_l(\tilde{\nu}) e^{-k_l t} + a_\infty(\tilde{\nu})$$

For each rate constant, an amplitude spectrum is obtained by global fit analysis. It corresponds to the difference spectrum of the states before and after the reaction in the case of well-separated reaction steps. In this work, one exponential was sufficient to describe the data, or in the case of reactions that were too fast, the photolysis spectra were examined instead. In the figures, negative-amplitude spectra $[-a_l(\tilde{\nu})]$ are shown, so that negative bands belong to the disappearing state and positive bands to the appearing state. An amplitude spectrum of the photolysis $a_0(\tilde{\nu})$ is calculated by

$$a_0(\tilde{\nu}) = a_\infty(\tilde{\nu}) - \sum_{l=1}^{n_r} a_l(\tilde{\nu})$$

RESULTS

Loss of More Than One Ankyrin Repeat Impairs the Phosphocholine Transferase Activity of AnkX. We examined the phosphocholination (PCylation) of Rab1b by different AnkX constructs with time-resolved fluorescence measurements and ESI-MS. Shortened AnkX constructs were created on the basis of the prediction of the location of ankyrin repeats as described previously.[25] Full length AnkX contains 12 ankyrin repeats, while slightly shortened $AnkX_{1-800}$ still contains 12 repeats and can be considered as the full length equivalent in this regard. All used constructs are listed in Supplementary Table 1. The PCylation assay based on tryptophan fluorescence of Rab1b was established previously.[43]

The apparent monoexponential fluorescence increase during PCylation of Rab1b with catalytic amounts of AnkX is a measure of the catalytic activity and was used to compare different AnkX constructs (Figure 1). While full length AnkX,

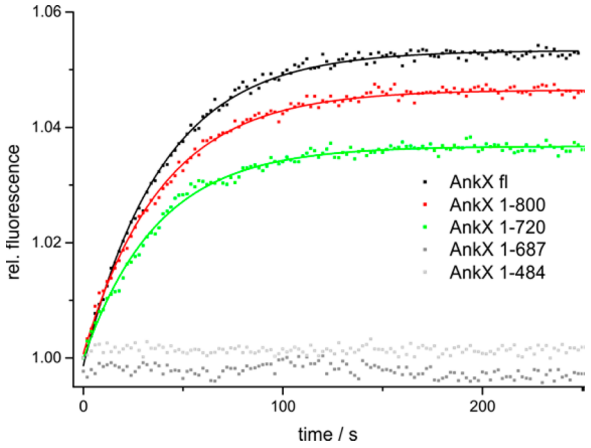

Figure 1. Phosphocholination of Rab1b·GDP monitored by tryptophan fluorescence (10 μM Rab1b, 400 μM CDP-choline, and 200 nM AnkX at 25 °C). Apparent reaction lifetimes from monoexponential fits are 39 ± 0.5 s for $AnkX_{fl}$, 35 ± 0.4 s for $AnkX_{1-800}$, and 37 ± 0.7 s for $AnkX_{1-720}$. AnkX constructs lacking more than two ankyrin repeats, such as $AnkX_{1-687}$ or shorter, have strongly reduced phosphocholinetransferase activity.

$AnkX_{1-800}$, and $AnkX_{1-720}$ exhibited essentially the same kinetics, virtually no fluorescence increase was observed for $AnkX_{1-687}$ and all shorter variants, including the published version, $AnkX_{1-484}$. $AnkX_{1-720}$ lacks two ankyrin repeats, while $AnkX_{1-687}$ already lacks three. However, $AnkX_{1-484}$ was previously shown to be able to PCylate Rab1b[25] and also to induce *in vivo* effects similar to those of the full length protein.[15] Indeed, we were able to confirm PCylation of Rab1b for all AnkX variants by ESI-MS (see Experimental Procedures for details and Supplementary Figure 4). Because a 1:1 AnkX:Rab1b ratio and an incubation time of 1 h were employed for ESI-MS measurements, while fluorescence measurements were finished after 5 min with 2 mol % AnkX, the apparent discrepancy between mass and fluorescence analyses can be explained. Thus, AnkX constructs lacking more than two ankyrin repeats suffer a drastic decrease in their ability to PCylate Rab1b. Nevertheless, the activity is not completely lost, as shown by ESI-MS (Supplementary Figure 4). The exact kinetics could not be determined, but the less active constructs can be estimated to be slowed by at least 2 orders of magnitude.

In addition to its transferase activity, AnkX is able to hydrolyze CDP-choline in a multiturnover reaction in the absence of Rab1b.[43] We investigated this reaction in a HPLC assay monitoring conversion of CDP-choline to CMP, which revealed that hydrolysis occurs in a manner independent of the number of ankyrin repeats (Supplementary Figure 5). Obviously, the catalytic center of AnkX is able to transfer the phosphocholine moiety to a water molecule, but a certain number of ankyrin repeats are required for the transfer to Rab1b. It is not clear how the ankyrin repeats contribute to the phosphocholine transferase activity of the FIC domain. Because the published AnkX structure includes only four ankyrin repeats,[25] we performed a structural alignment of $AnkX_{1-484}$ with AnkyrinR (Figure 2).[44] The alignment reveals that the

DOI: 10.1021/acs.biochem.6b00524
Biochemistry 2016, 55, 4375−4385

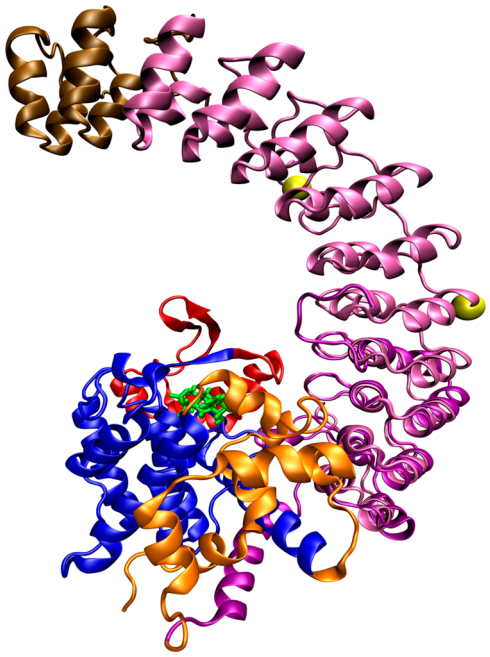

Figure 2. Structural alignment of $AnkX_{1-484}$ (PDB entry 4BES) with AnkyrinR (PDB entry 1N11), showing the probable shape of the complete ankyrin repeat region of $AnkX_{1-800}$: blue, FIC domain; orange, CMP-binding domain; red, insert domain; purple, ankyrin repeats. The overlaid ankyrin repeats are colored light purple, while the last two repeats colored brown were found to be critical for the enzymatic activity of AnkX. Bound CDP-choline is colored green. Approximate locations of autophosphocholination sites of AnkX (Ser521 and Thr620) based on the sequence alignment of AnkX and AnkyrinR are shown as yellow spheres.

ankyrin repeats most probably adopt a clamplike conformation around the FIC domain. The manner in which AnkX interacts with its substrate Rab1b is not known, but the repeats might enhance the binding of Rab1b in the correct orientation for efficient catalysis. Surprisingly, the loss of two ankyrin repeats does not seem to be a drastic shortening of the clamp (brown in Figure 2), but obviously, a crucial interaction interface must be located in this region of AnkX. It is unlikely that the last two ankyrin repeats directly contribute any residues for catalysis because they are not located in the proximity of the active site.

Autophosphocholination within the Ankyrin Repeats Does Not Influence the Catalytic Activity. Previous studies suggested different locations of autoPCylation of AnkX as outlined in the introductory section.[25,43] Different conclusions have been drawn concerning, i.e., phosphocholination of the catalytic His229. Therefore, we examined in detail which AnkX constructs are able to undergo autoPCylation, which residues are modified, and if multiple modification occurs. AnkX constructs were incubated with a large excess of CDP-choline and analyzed by ESI-MS. All examined constructs that are longer than residues 1−527 were found to be doubly PCylated; $AnkX_{1-527}$ was found to be PCylated five times, and shorter constructs were not PCylated (Supplementary Table 1). The found threshold is in agreement with the results of Campanacci et al., who observed PCylation of full length AnkX but not of $AnkX_{1-484}$ with Western blotting.[25] Therefore, the accumulating PCylated species does not represent PCylation of the active site histidine. However, one should not expect the accumulation of this state because phosphohistidine derivatives are generally unstable[45] and also because AnkX efficiently hydrolyzes CDP-choline under multiple-turnover conditions in the absence of a GTPase substrate.

The fact that, in the case of fully active AnkX constructs, the accumulating species was doubly PCylated led us to further investigate which residues are modified, if the modification occurs intra- or intermolecularly, and if it influences the enzymatic activity of AnkX. Shotgun nano LC−MS analyses revealed that Ser521, Thr620, and Thr943 are PCylated in full length AnkX (Supplementary Figure 6). Interestingly, the MS data with different AnkX constructs (Supplementary Table 1) did not support strict localization of PCylated residues to this region of the protein. The shotgun analyses were performed with full length AnkX, while shorter constructs appear to have a different specificity for autoPCylation due to varying conformational flexibility and accessibility.

Because we mainly employed $AnkX_{1-800}$, which has the same catalytic activity as the full length protein, we investigated the impact of mutation of the identified autophosphocholination sites Ser521 and Thr620, but not Thr943. Mutation of Ser521 and Thr620 to alanine did not affect the catalytic activity of AnkX in the fluorescence assay (Supplementary Figure 7), indicating that autoPCylation is not relevant in this respect. Moreover, this is in line with the finding that constructs shorter than $AnkX_{1-720}$ are significantly impaired despite having the

Scheme 1. Photochemical Reaction of Caged Compounds (A) npeCDP and (B) phpCDP

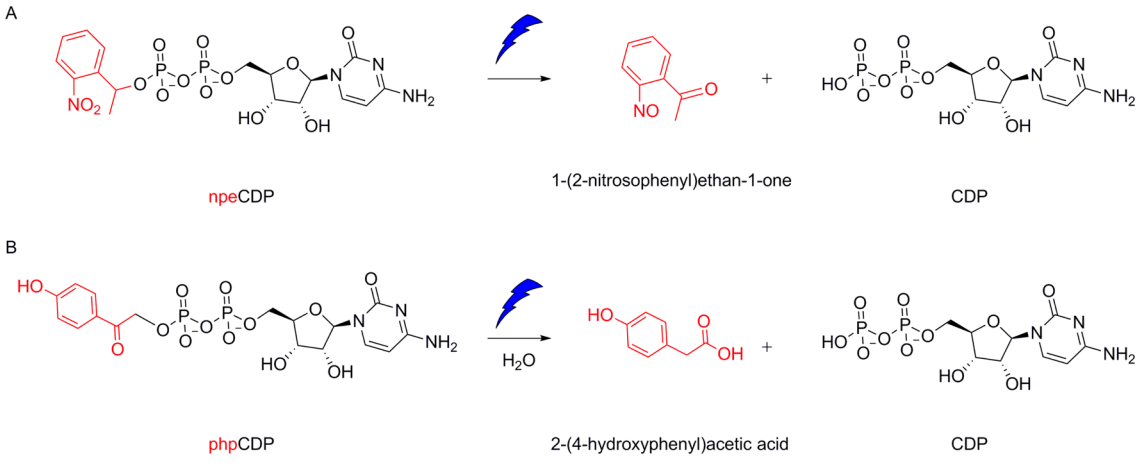

DOI: 10.1021/acs.biochem.6b00524
Biochemistry 2016, 55, 4375−4385

autoPCylation sites Ser521 and Thr620. Furthermore, incubation of $AnkX_{1-800}$H229A with catalytic amounts of wild-type AnkX did not result in PCylation (Supplementary Table 1). This means that the AnkX protein is able to perform only an intramolecular modification but does not recognize other AnkX molecules as substrates. Also, according to sequence alignment of AnkX with AnkyrinR, Ser521 and Thr620 can be mapped on the AnkyrinR structure facing the solvent and not the active site of the FIC domain, consistent with this observation. Unless autoPCylation is involved in an unknown protein interaction, it appears to be a byproduct of AnkX-mediated hydrolysis of CDP-choline, and thus, it is less surprising that autoPCylation of shorter constructs such as $AnkX_{1-527}$ is less specific.

Resolving the AnkX-Catalyzed Modification of Rab1b with FTIR Spectroscopy. Because biochemical data did not provide a clear picture of the catalytic mechanism, especially regarding a possible transient phosphocholination of the catalytic His229, we employed time-resolved FTIR difference spectroscopy. To trigger the fast enzymatic reaction of AnkX with a laser pulse, we synthesized novel caged compounds based on the AnkX substrates CDP-choline and CDP (see Experimental Procedures and Supplementary Figures 1−3). The quantum yield of phpATP is 0.37 with a rate constant of 5.5×10^8 s^{-1} according to Givens and Lee.[46] In the case of npeATP, a quantum yield of 0.63 and a rate constant of 86 s^{-1} have been described in the literature.[34] Because the employed CDP analogues have the same photochemical mechanism, similar quantum yields and rate constants can be assumed. The release time of the nucleotides is significantly faster than the time resolution of our measurements and can therefore be neglected. Typical absorbance spectra of 1-(2-nitro)-phenylethyl-CDP-choline (npeCDP-choline) and phpCDP are shown in Supplementary Figure 8. Furthermore, the photochemical reaction of npeCDP and phpCDP is presented in Scheme 1. npeCDP-choline was prepared but found to be a substrate for AnkX despite bearing the caging group. Although the compound could be photolyzed, degradation of npeCDP-choline prior to photolysis was observed in the presence of AnkX (Supplementary Figure 9). FTIR samples require sufficient stabilization times before the measurement can be started to eliminate baseline drifts, and therefore, npeCDP-choline could not be utilized to obtain meaningful results. Thus, we synthesized caged CDP derivatives bearing either npe or 4-hydroxyphenacyl (php) groups: npeCDP provides good thermal stability for use at physiological temperatures, while phpCDP has a faster photolysis reaction, allowing a higher temporal resolution to be achieved at lower temperatures. CDP, similar to CDP-choline, is also a suitable substrate for modification of Rab1b at Ser76 by AnkX,[43] and the conversion of the phosphoanhydride group into the phosphorylester can be expected to follow the same chemical mechanism as for CDP-choline. However, modification of Rab1b was found to proceed with CDP slower than with CDP-choline, which could be due to different charges at the β-phosphate, possibly limiting the comparability to the natural substrate. Neither npeCDP nor phpCDP was degraded by AnkX unlike npeCDP-choline, permitting their use for time-resolved studies. Moreover, we found that CDP is not hydrolyzed by AnkX in the absence of Rab1b (Supplementary Figure 5). Therefore, this reaction would not interfere with the actual modification of Rab1b in FTIR measurements, eliminating the need to separate parallel reactions during analysis.

Because FTIR difference spectroscopy requires millimolar protein concentrations, suitable AnkX constructs had to be chosen to ensure that the investigated protein is stable and active under such conditions. Therefore, only $AnkX_{1-800}$ and $AnkX_{1-484}$ could be employed for FTIR measurements, intermediate constructs being surprisingly less stable under FTIR conditions. We were able to resolve two distinct reaction steps using these constructs. $AnkX_{1-800}$ modified Rab1b as was expected from previous data. Also, low-temperature measurements with $AnkX_{1-800}$ revealed an additional reaction rate preceding the phosphoryl transfer reaction. $AnkX_{1-484}$ was not able to modify Rab1b on the investigated time scale but still performed the first reaction step. The lower molecular mass of $AnkX_{1-484}$ allowed spectra with intensity greater than that of the spectra of $AnkX_{1-800}$ to be recorded, revealing additional details, as will be discussed later.

The k_{cat} value for the phosphocholination reaction was previously determined to be 27 ± 2.3 s^{-1} at 25 °C,[21] and rapid-scan FTIR does not have sufficient time resolution for such kinetics. Therefore, we obtained difference spectra of the modification of Rab1b by $AnkX_{1-800}$ and CDP and, but not its kinetics. The difference spectra of the phosphoryl transfer reaction were calculated by subtraction of the photolysis spectra in the presence and absence of Rab1b (Supplementary Figure 10). Band assignments were performed with isotopically labeled caged CDP derivatives by calculating double-difference spectra. Figure 3 shows that CMP is formed in the reaction of AnkX

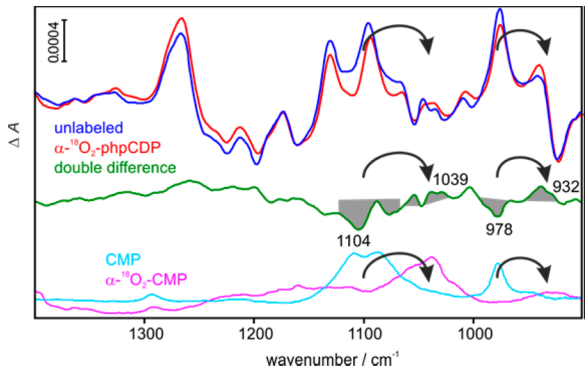

Figure 3. Assignment of the α-phosphate bands in the infrared spectra of the phosphorylation reaction using unlabeled (blue) and α-$^{18}O_2$-labeled phpCDP (red). Negative bands belong to free Rab1b and CDP bound to AnkX, and positive bands belong to Rab1b-P_i and CMP. The double difference spectrum (labeled − unlabeled) is colored in green. The α-phosphate vibrations of emerging CMP are detected at 1104 and 978 cm^{-1}. For comparison, the spectra of CMP and α-$^{18}O_2$-CMP are shown below. Note that the α-phosphate vibrations of disappearing CDP overlap with the CMP bands around 1100 cm^{-1} and cannot be clearly resolved as indicated by numerous gray shaded bands in the double-difference spectrum.

and Rab1b with CDP. α-$^{18}O_2$ labeling induced shifts of the positive bands at 978 and 1104 cm^{-1}. These bands belong to the $\nu_s(PO_3^{2-})$ and $\nu_{as}(PO_3^{2-})$ vibrations of CMP, respectively,[47] which is best illustrated by the direct comparison of absorbance spectra of CMP and α-$^{18}O_2$-CMP (Figure 3). Furthermore, the difference spectrum of the reaction confirms the phosphorylation of Rab1b, as seen with β-$^{18}O_4$ labeling (Figure 4). The phosphorylated side chain of Ser76 is chemically identical to the phosphate group of CMP, and therefore, the same bands can be found. The symmetric vibration of phosphorylated Ser76 is clearly detected at 978

DOI: 10.1021/acs.biochem.6b00524
Biochemistry 2016, 55, 4375−4385

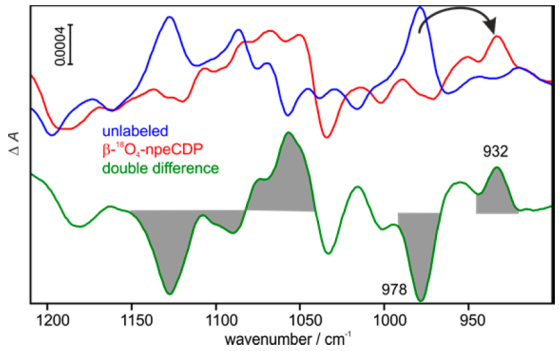

Figure 4. Assignment of the β-phosphate bands in the infrared amplitude spectra of the phosphorylation reaction using unlabeled (blue) and β-$^{18}O_4$-labeled npeCDP (red). Negative bands belong to free Rab1b and CDP bound to AnkX, and positive bands belong to Rab1b-P_i and CMP. The double-difference spectrum (labeled − unlabeled) is colored green. The phosphoserine vibration is detected at 978 cm^{-1}. Like CMP, the phosphoserine is expected to have bands in the region around 1100 cm^{-1}, which overlap with β-CDP bands. This is indicated by numerous gray shaded bands in the double-difference spectrum.

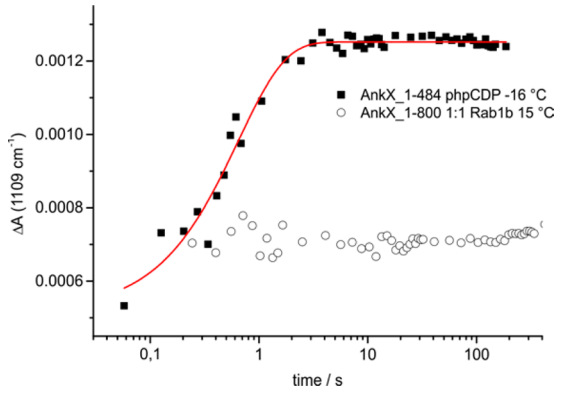

Figure 5. Kinetics of the precatalytic conformational change of AnkX bound to CDP. Time-dependent absorbance changes of a marker band in the phosphate region at 1109 cm^{-1}. Time traces after photolysis of phpCDP for $AnkX_{1-484}$ at −16 °C are shown as black squares, and those for $AnkX_{1-800}$ in the presence of Rab1b at 15 °C are shown as circles. The red line represents a monoexponential fit that yields a lifetime of 600 ± 40 ms. The phosphorylation reaction with Rab1b had to be performed at 15 °C, where this early reaction could not be resolved. In principle, this reaction rate could also be resolved with $AnkX_{1-800}$ at −16 °C, but with a much worse signal-to-noise ratio.

cm^{-1}; the asymmetric vibration band overlaps with disappearing bands of the β-phosphate of CDP, and both bands cannot be clearly assigned in the double-difference spectrum (Figure 4). The difference bands associated with the phosphates dominate the spectrum, but protein bands in the amide region can be detected, as well (Supplementary Figure 10). Because this difference spectrum represents the changes only between the initial and final states of the reaction, the bands may reflect subtle conformational changes in Rab1b as previously detected for adenylylation.[11] No intermediate states involving AnkX are resolved here, as described in the case of the previously measured difference spectra of Rab1b adenylylation by DrrA.[11] The data confirm that AnkX catalyzes the phosphoryl transfer reaction under FTIR conditions, but moreover, we were able to identify an important precatalytic step at lower temperatures as discussed below.

Precatalytic Conformational Change of AnkX. An additional reaction rate was revealed in low-temperature measurements (600 ± 40 ms, −16 °C) with AnkX using phpCDP (Figure 5). This rate did not depend on the presence of Rab1b, indicating that it involves an interaction of AnkX with CDP that precedes the phosphoryl transfer reaction. Supplementary Figure 11 shows the corresponding amplitude spectrum in the phosphate region. The overall amplitude is similar to the spectrum of the phosphoryl transfer reaction (Supplementary Figure 10). Therefore, the rate is unlikely to represent a minor rearrangement but rather may reflect the binding of CDP to AnkX, considering that AnkX does not bind the caged compounds (see Experimental Procedures). The largest bands in the phosphate region are a negative band at 1129 cm^{-1} and a positive band at 1109 cm^{-1}. The asymmetric vibration of the β-phosphate of nucleotide diphosphates is found at ∼1123 cm^{-1}, and its position in the binding pocket will shift depending on the nature of the interactions with the protein.[48] However, β-phosphate-labeled phpCDP was not available to us for direct band assignment. Therefore, we can only tentatively assign the band at 1129 cm^{-1} to the β-phosphate of CDP undergoing an environmental change. α-$^{18}O_2$ labeling revealed only small band shifts (Supplementary Figure 11), meaning that the corresponding vibrations are not strongly affected. Small shifts are detected in the region of the aforementioned negative band at 1129 cm^{-1} and the positive band at 1109 cm^{-1}. This reflects the combinational nature of this vibration, but the contribution of the α-phosphate appears to be small. Therefore, we can conclude that the conformational change does not strongly influence the α-phosphate. Also, it is clear that CDP is still present in this state because no CMP band is detected, which would appear at 979 cm^{-1}.

His229 Is Locked in a Deprotonated State for Nucleophilic Attack. Next, we studied the influence of mutations on the precatalytic rate and uncovered the molecular details of the changes in the CDP-binding site. In particular, we were interested in the role of His229 and the relevance of the precatalytic change for the overall reaction. The spectral region between 1700 and 1800 cm^{-1} caught our attention because of the presence of several clear difference bands (Supplementary Figures 11 and 12 and Figure 6). Such bands indicate protonation or environmental changes of carboxylic acids[49] and, to the best of our knowledge, have been observed only recently once in a phosphoryl transfer reaction, though not in the active site of the protein.[50] Three carboxylic acids can be found in the close proximity of CDP-choline/CDP and the catalytic histidine[25] (Figure 7): Asp233, Asp265, and Glu226. Of these, Asp233 is thought to coordinate the magnesium ion, and the other two residues are located in the vicinity of the choline moiety. To confirm proton transfer, we performed measurements in deuterium oxide (Figure 6B). The data indicate changes of two carboxylic acid residues, of which one is solvent-exposed and undergoes protonation, as shown by a clear shift of the positive band from 1726 to 1721 cm^{-1} and the lack of the corresponding shifting negative COOH band (Figure 6B). Another protonated carboxylic acid appears to be water inaccessible and undergoes an environmental change (bands at 1761 and 1745 cm^{-1} that are not influenced by D_2O). Thus, the latter carboxylic acid is located farther from the active site and is water inaccessible but interacts with Glu226 and might therefore be Asp265.

Further assignment of residues involved in proton transfer is performed by using mutagenesis-induced changes in the

DOI: 10.1021/acs.biochem.6b00524
Biochemistry 2016, 55, 4375−4385

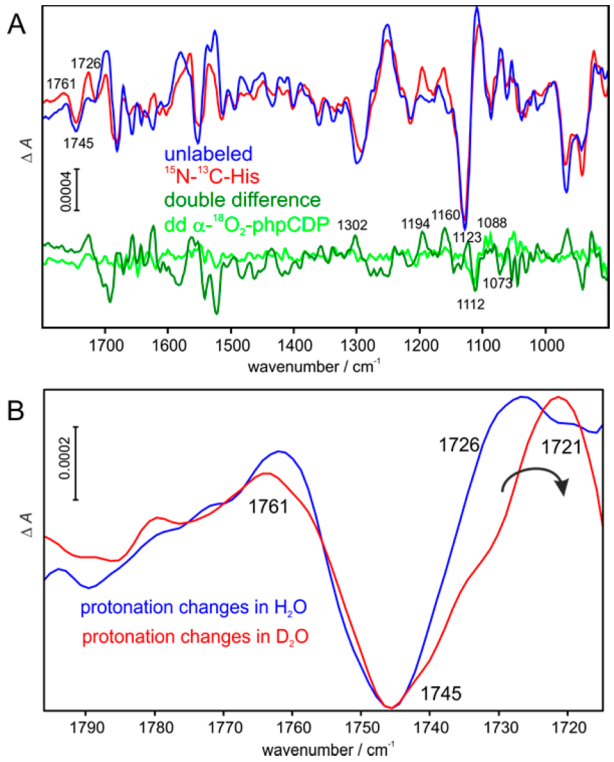

Figure 6. Assignment of protonation changes in the precatalytic conformational change of AnkX. (A) Assignment of histidine bands using unlabeled (blue) and $^{15}N_3$- and $^{13}C_6$-labeled (red) AnkX. Negative bands belong to the state directly after photolysis of caged CDP, and positive bands belong to the precatalytic state. The double-difference spectrum is colored green, and the double-difference spectrum with α-$^{18}O_2$-phpCDP is colored light green as an example in which virtually no changes are detected. The band pattern in the double-difference spectrum shows deprotonation of histidine [e.g., positive bands at 1194 and 1160 cm^{-1} and negative band at 1112 cm^{-1} (cf. Supplementary Figure 14 for all histidine bands at different pH values)]. (B) Isotopic shift of carboxylic acids bands induced by D_2O. A carboxylate residue undergoes protonation (band shift from 1726 to 1721 cm^{-1}). A protonated carboxylic acid, which is water inaccessible, undergoes an environmental change (1761 and 1745 cm^{-1}).

carboxyl band pattern. Therefore, we investigated the activity and spectral changes of the D233N, D265N, and E226Q mutants with fluorescence, HPLC, and FTIR. The activity of D233N was completely lost as seen in the tryptophan fluorescence PCylation assay (Supplementary Figure 7). Also, no spectra of the precatalytic conformational change could be obtained with FTIR. This is in line with the expected role of Asp233 in the coordination of the magnesium ion and its strict requirement for catalysis. A carboxylate side chain interacting with a cation is unlikely to undergo a protonation.[51] D265N and E226Q were impaired in their PCylation activity, indicating a role in catalysis (Supplementary Figure 7). While E226Q showed a 10-fold decrease in activity as compared to that of wild-type AnkX, D265N was so heavily impaired that it was impossible to obtain fluorescence data for a reliable fit (Supplementary Figure 7). Although both mutants retained PCylation activity to a certain degree, none of them were able to autohydrolyze CDP-choline as determined by the HPLC assay (Supplementary Figure 5). The rate constant of the precatalytic conformational change observed in FTIR correlates with the PCylation activity and was similarly diminished in both mutants and not visible in D233N. Supplementary Figure 12 compares the difference spectra of the precatalytic conformational change in wild-type AnkX and AnkX E226Q. The mutation leads to the almost complete disappearance of difference bands in the carboxylic acid region between 1700 and 1800 cm^{-1}. This band, as discussed above, suggests that one carboxylate residue undergoes protonation. Glu226 and Asp265 are clearly involved in this proton transfer, although the data do not allow us to determine which of the two residues is protonated.

Next, we asked what is the source of the appearing proton. We hypothesized that the catalytic His229 could be involved in the observed proton transfer because the occurrence of the precatalytic proton transfer directly correlated with the phosphocholine transferase activity of AnkX. Furthermore, the precatalytic conformational change could not be observed with the H229A mutant, underlining the role of this residue. We isolated [$^{15}N_3$,$^{13}C_6$]His-labeled AnkX$_{1-484}$, confirmed >98% incorporation of the labeled amino acid in the protein by MS/MS spectrometry (Supplementary Figure 13), and analyzed the band shifts in the difference spectrum of the proton transfer (Figure 6A). Numerous band shifts were observed in the double-difference spectrum, as expected for histidine. The assignment was made on the basis of on the literature[52] and additional reference measurements of histidine at different pH values (Supplementary Figure 14). The band pattern in the double-difference spectrum is consistent with deprotonation of histidine, which is exemplified by the most prominent positive bands at 1194 and 1160 cm^{-1} and the negative band at 1112 cm^{-1}. Considering that the previously discussed changes in the precatalytic rate could be assigned to moieties in and around the catalytic site, we conclude that the observed histidine deprotonation most likely belongs to the catalytic His229. The deprotonation creates an uncharged state of the imidazole side chain necessary for the execution of a nucleophilic attack. While the initial protonated state of His229, which the catalytic site is able to adopt, may be induced by our experimental conditions such as the use of a php-caged compound, AnkX needs to maintain His229 in the deprotonated state to ensure enzymatic activity. In the CDP-bound form, stabilization of this state of His229 appears to be ensured by the network comprising Glu226 and Asp265, explaining the impact of E226Q and D265N on catalytic efficiency. One of these two carboxylate residues accepts the proton originating from His229 (Supplementary Figure 12 and Figure 7), but the protonation pattern in the CDP-choline-bound form may be different from the present charge of the choline group.[25]

DISCUSSION

Our combined biochemical and spectroscopic data give detailed information about the molecular mechanism of the phosphoryl transfer reaction catalyzed by AnkX. Previous studies suggested differing mechanisms of phosphoryl transfer and roles of His229: a ping-pong mechanism or a concerted mechanism. These conclusions were drawn from steady-state kinetics[43] and structural studies combined with biochemical data,[25] respectively. The important question is whether the catalytic histidine is transiently phosphocholinated and if automodification of AnkX is relevant with respect to enzymatic activity. We find that it is crucial to distinguish between autophosphocholination in the ankyrin repeats and within the FIC domain and to correlate this with catalytic activity.

Combination of time-resolved fluorescence measurements, HPLC, and ESI-MS analytics allowed us to precisely determine

DOI: 10.1021/acs.biochem.6b00524
Biochemistry 2016, 55, 4375−4385

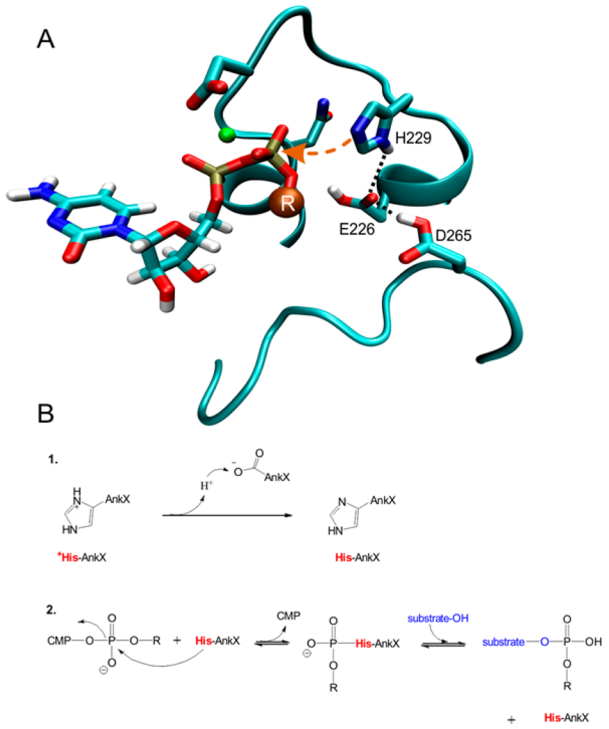

Figure 7. Proposed reaction mechanism of AnkX. (A) Structural view of the active site based on the crystal structures of $AnkX_{1-484}$.[25] The blue sphere marked as "R" at the β-phosphate represents the group that will be transferred to the Rab GTPase. The protonation states of His229, Glu226, and Asp265 are depicted as determined by FTIR. While it is possible that both acids are in the protonated form, the possibility that the proton is further transferred to an unidentified residue outside of the active site cannot be excluded. In both scenarios, His229 is stabilized in this specific protonation state by the hydrogen bond network. Thus, the nucleophilic attack on the β-phosphate of the nucleotide can occur (dashed arrow). (B) Scheme for the ping-pong mechanism illustrating the reaction steps. First, His229 is deprotonated by a carboxylate. Second, a nucleophilic attack on the β-phosphate takes place.

the activity of AnkX variants with different numbers of ankyrin repeats. AnkX constructs shorter than residues 1−720 are heavily impaired in their catalytic activity, which, however, is not related to the autophosphocholination sites present in the ankyrin repeats (Figure 1 and Supplementary Table 1). Previously, $AnkX_{1-484}$ was described as having full catalytic activity based on Western blot data.[25] Such experiments involve long incubation times, and we also observed modification of Rab1b by $AnkX_{1-484}$ under similar conditions with ESI-MS. However, care should be taken because long incubation times prior to blot analysis mask the real activity that we revealed with the sensitive fluorescence assay. Thus, a minimum of 10 ankyrin repeats is required for full enzymatic activity. It is not yet clear what the exact role of the ankyrin repeats is because no structural data of AnkX in complex with a substrate are available. It is conceivable that the repeats contribute to the recognition of the substrate or stabilize the FIC domain. Furthermore, autophosphocholination of serine and threonine residues within the ankyrin repeats appears to be an unspecific intramolecular modification and is not relevant for enzymatic activity (Supplementary Figure 7 and Supplementary Table 1).

To investigate the molecular mechanism in detail, we synthesized novel CDP-based caged compounds with specific isotopic labels to address a class of enzymes that has been previously not been accessible by time-resolved spectroscopy. With this technique, we were able to resolve a precatalytic deprotonation of histidine that is likely His229 in the active site. A hydrogen bond network around the active site is present to lock the histidine in this state. Hence, the deprotonated histidine is primed for nucleophilic attack on the transferred phosphate.

We propose the following reaction mechanism of AnkX based on the combined data (Figure 7). AnkX with His229 stabilized in the deprotonated form binds CMP bearing the transferred group. His229 performs a nucleophilic attack on the β-phosphate, resulting in a reactive transient phosphohistidine species. After dissociation of CMP, the transferred group is coupled to the substrate, which can be a Rab GTPase or a water molecule in the case of autohydrolysis. While our measurements cannot directly capture the possible transient phosphohistidine species, our results are compatible with this type of mechanism, and previous observations in the literature tend to rule out a concerted mechanism. The crystal structure of AnkX with various ligands supports a ping-pong mechanism because no water molecules were present between the transferred phosphate moiety and His229, which would be required for a concerted mechanism. Also, a water molecule would be sterically hindered in the space between these residues.[25] Additionally, one needs to consider if the substrate, such as Rab1b, would be able to bind in an orientation allowing an attack on the phosphohistidine. While the crystal structure of product-bound IpbA[14] clearly excludes a ping-pong mechanism for the adenylylation of Cdc42 for sterical reasons, the presence of an insert domain in AnkX implies a different binding modality for Rab1b, which could be compatible with a ping-pong mechanism. Furthermore, the possibility that phosphohistidine derivatives are high-energy compounds and therefore unlikely to accumulate and be detected by ESI-MS or Western blotting needs to be considered. Therefore, the absence of a detectable stable phosphocholination of $AnkX_{1-484}$ does not imply that a phosphocholinated histidine intermediate does not occur, as previously interpreted,[25] especially given the low enzymatic activity of this construct. In contrast, double-reciprocal plots of steady-state kinetics clearly indicated a ping-pong mechanism.[43] Ultimately, deeper insights could be obtained from a structure of AnkX in complex with a GTPase, which remains unresolved so far.

Posttranslational modifications such as nucleotidylation and phosphocholination are emerging modifications for regulation of protein functions, especially utilized by bacterial pathogens. Currently, the spectrum of substrates mainly encompasses GTPases, but many additional targets are likely to be identified by MS-based screens employing chemically modified substrates and PTM-specific antibodies.[53] Furthermore, FIC domain-containing proteins are present in many genomes, including the HYPE protein in humans,[8,12] which possesses adenylylation activity. Therefore, previously uncharacterized enzymes are likely to emerge in all kingdoms of life. Because FIC domains can catalyze a variety of reactions using different nucleotide substrates, and these reactions can in some cases be catalyzed by structurally unrelated proteins, such as adenylylation by DrrA, we can expect a variety of intriguing reactions to be discovered. Here, we shed light on the molecular processes underlying phosphocholination, and recently, we elucidated the reaction mechanism of DrrA[11] using a similar methodology with different caged nucleotides. Our approach, including development of new caged compounds, will be useful for future

DOI: 10.1021/acs.biochem.6b00524
Biochemistry 2016, 55, 4375−4385

investigations of diverse reactions of regulatory or pathologically relevant proteins involving nucleotides such as ATP, GTP, CDP-choline, or UDP-glucose.

■ ASSOCIATED CONTENT

Supporting Information

The Supporting Information is available free of charge on the ACS Publications website at DOI: 10.1021/acs.biochem.6b00524.

Overview of caged compounds (Supplementary Figure 1), synthesis of [β-$^{18}O_4$]npe-CDP (Supplementary Figure 2), synthesis of [α-$^{18}O_2$]php-CDP (Supplementary Figure 3), ESI-MS spectra of PCylated Rab1b (Supplementary Figure 4), ESI-MS analysis of AnkX autoPCylation (Supplementary Table 1), hydrolysis of CDP-choline or CDP by AnkX monitored by HPLC (Supplementary Figure 5), shotgun nano LC−MS data for the identification of autophosphocholination sites in AnkX (Supplementary Figure 6), PCylation of Rab1b·GDP monitored by tryptophan fluorescence (Supplementary Figure 7), absorbance spectra of the caged compound (Supplementary Figure 8), photolysis and degradation of npeCDP-choline (Supplementary Figure 9), calculation of the difference spectrum of the Rab1b phosphorylation by AnkX (Supplementary Figure 10), assignment of the α-phosphate bands in the infrared spectra of the precatalytic conformational change of AnkX (Supplementary Figure 11), comparison of the amplitude spectra of the precatalytic conformational change (Supplementary Figure 12), MS/MS spectra of [$^{13}C_6$,$^{15}N_3$]His-labeled AnkX (Supplementary Figure 13), and ATR-FTIR spectra of histidine (Supplementary Figure 14) (PDF)

■ AUTHOR INFORMATION

Corresponding Authors

*E-mail: gerwert@bph.rub.de.
*E-mail: carsten.koetting@rub.de.

Present Address

[‖]K. Gavriljuk and H. Seidel: Department of Systemic Cell Biology, Max Planck Institute of Molecular Physiology, Otto-Hahn-Strasse 11, 44227 Dortmund, Germany.

Author Contributions

K. Gavriljuk and J. Schartner contributed equally to this work.

Funding

This work was performed in the framework of SFB 642 (German Research Foundation DFG, Sonderforschungsbereich 642, Projekt A1). R.P.Z. and C.D. thank the Ministry for Innovation, Science and Research of the Federal State of Northrhine-Westphalia for financial support. C.H. thanks the Knut and Alice Wallenberg foundation (Sweden) for generous support.

Notes

The authors declare no competing financial interest.

■ ACKNOWLEDGMENTS

We thank K. Mechtler for providing access to the ptmRS algorithm. We thank K. Marcus and C. Lindemann for the analysis of the isotopically labeled AnkX and D. Onidas for the vibrational data of isolated histidine compounds. Furthermore, we thank Aymelt Itzen for the AnkX full length plasmid and for helpful discussions.

■ ABBREVIATIONS

npeCDP, 1-(2-nitro)phenylethyl-cytidinediphosphate; PDB, Protein Data Bank; phpCDP, *p*-hydroxyphenacyl-cytidinediphosphate.

■ REFERENCES

(1) Berger, K. H., Merriam, J. J., and Isberg, R. R. (1994) Altered intracellular targeting properties associated with mutations in the Legionella pneumophila dotA gene. *Mol. Microbiol. 14*, 809−822.

(2) Marra, A., Blander, S. J., Horwitz, M. A., and Shuman, H. A. (1992) Identification of a Legionella pneumophila locus required for intracellular multiplication in human macrophages. *Proc. Natl. Acad. Sci. U. S. A. 89*, 9607−9611.

(3) Horwitz, M. A. (1983) Formation of a novel phagosome by the Legionnaires' disease bacterium (Legionella pneumophila) in human monocytes. *J. Exp. Med. 158*, 1319−1331.

(4) Heidtman, M., Chen, E. J., Moy, M.-Y., and Isberg, R. R. (2009) Large-scale identification of Legionella pneumophila Dot/Icm substrates that modulate host cell vesicle trafficking pathways. *Cell. Microbiol. 11*, 230−248.

(5) Isberg, R. R., O'Connor, T. J., and Heidtman, M. (2009) The Legionella pneumophila replication vacuole: making a cosy niche inside host cells. *Nat. Rev. Microbiol. 7*, 13−24.

(6) Zhen, Y., and Stenmark, H. (2015) Cellular functions of Rab GTPases at a glance. *J. Cell Sci. 128*, 3171−3176.

(7) Mukherjee, S., Liu, X., Arasaki, K., McDonough, J., Galán, J. E., and Roy, C. R. (2011) Modulation of Rab GTPase function by a protein phosphocholine transferase. *Nature 477*, 103−106.

(8) Roy, C. R., and Cherfils, J. (2015) Structure and function of Fic proteins. *Nat. Rev. Microbiol. 13*, 631−640.

(9) Feng, F., Yang, F., Rong, W., Wu, X., Zhang, J., Chen, S., He, C., and Zhou, J.-M. (2012) A Xanthomonas uridine 5′-monophosphate transferase inhibits plant immune kinases. *Nature 485*, 114−118.

(10) Garcia-Pino, A., Zenkin, N., and Loris, R. (2014) The many faces of Fic: structural and functional aspects of Fic enzymes. *Trends Biochem. Sci. 39*, 121−129.

(11) Gavriljuk, K., Schartner, J., Itzen, A., Goody, R. S., Gerwert, K., and Kötting, C. (2014) Reaction mechanism of adenylyltransferase DrrA from Legionella pneumophila elucidated by time-resolved fourier transform infrared spectroscopy. *J. Am. Chem. Soc. 136*, 9338−9345.

(12) Hedberg, C., and Itzen, A. (2015) Molecular perspectives on protein adenylylation. *ACS Chem. Biol. 10*, 12−21.

(13) Yarbrough, M. L., Li, Y., Kinch, L. N., Grishin, N. V., Ball, H. L., and Orth, K. (2009) AMPylation of Rho GTPases by Vibrio VopS disrupts effector binding and downstream signaling. *Science 323*, 269−272.

(14) Xiao, J., Worby, C. A., Mattoo, S., Sankaran, B., and Dixon, J. E. (2010) Structural basis of Fic-mediated adenylylation. *Nat. Struct. Mol. Biol. 17*, 1004−1010.

(15) Pan, X., Lührmann, A., Satoh, A., Laskowski-Arce, M. A., and Roy, C. R. (2008) Ankyrin repeat proteins comprise a diverse family of bacterial type IV effectors. *Science 320*, 1651−1654.

(16) Müller, M. P., Peters, H., Blümer, J., Blankenfeldt, W., Goody, R. S., and Itzen, A. (2010) The Legionella effector protein DrrA AMPylates the membrane traffic regulator Rab1b. *Science 329*, 946−949.

(17) Wittinghofer, A., and Vetter, I. R. (2011) Structure-function relationships of the G domain, a canonical switch motif. *Annu. Rev. Biochem. 80*, 943−971.

(18) Casey, P. J., and Seabra, M. C. (1996) Protein prenyltransferases. *J. Biol. Chem. 271*, 5289−5292.

(19) Wu, Y.-W., Goody, R. S., Abagyan, R., and Alexandrov, K. (2009) Structure of the disordered C terminus of Rab7 GTPase induced by binding to the Rab geranylgeranyl transferase catalytic

DOI: 10.1021/acs.biochem.6b00524
Biochemistry 2016, 55, 4375−4385

complex reveals the mechanism of Rab prenylation. *J. Biol. Chem. 284*, 13185−13192.
(20) Alory, C., and Balch, W. E. (2001) Organization of the Rab-GDI/CHM superfamily: the functional basis for choroideremia disease. *Traffic 2*, 532−543.
(21) Goody, P. R., Heller, K., Oesterlin, L. K., Müller, M. P., Itzen, A., and Goody, R. S. (2012) Reversible phosphocholination of Rab proteins by Legionella pneumophila effector proteins. *EMBO J. 31*, 1774−1784.
(22) Gavriljuk, K., Itzen, A., Goody, R. S., Gerwert, K., and Kotting, C. (2013) Membrane extraction of Rab proteins by GDP dissociation inhibitor characterized using attenuated total reflection infrared spectroscopy. *Proc. Natl. Acad. Sci. U. S. A. 110*, 13380−13385.
(23) Wheeler, D. B., Zoncu, R., Root, D. E., Sabatini, D. M., and Sawyers, C. L. (2015) Identification of an oncogenic RAB. *Science 350*, 211−217.
(24) Heller, K., Ochtrop, P., Albers, M. F., Zauner, F. B., Itzen, A., and Hedberg, C. (2015) Covalent Protein Labeling by Enzymatic Phosphocholination. *Angew. Chem., Int. Ed. 54*, 10327−10330.
(25) Campanacci, V., Mukherjee, S., Roy, C. R., and Cherfils, J. (2013) Structure of the Legionella effector AnkX reveals the mechanism of phosphocholine transfer by the FIC domain. *EMBO J. 32*, 1469−1477.
(26) Kötting, C., and Gerwert, K. (2005) Proteins in action monitored by time-resolved FTIR spectroscopy. *ChemPhysChem 6*, 881−888.
(27) Gerwert, K. (1992) Molecular reaction mechanism of photosynthetic proteins as determined by FTIR-spectroscopy. *Biochim. Biophys. Acta, Bioenerg. 1101*, 147−153.
(28) Schartner, J., Güldenhaupt, J., Mei, B., Rögner, M., Muhler, M., Gerwert, K., and Kötting, C. (2013) Universal method for protein immobilization on chemically functionalized germanium investigated by ATR-FTIR difference spectroscopy. *J. Am. Chem. Soc. 135*, 4079−4087.
(29) Noguchi, T. (2015) Fourier transform infrared difference and time-resolved infrared detection of the electron and proton transfer dynamics in photosynthetic water oxidation. *Biochim. Biophys. Acta, Bioenerg. 1847*, 35−45.
(30) Kuhne, J., Eisenhauer, K., Ritter, E., Hegemann, P., Gerwert, K., and Bartl, F. (2015) Early Formation of the Ion-Conducting Pore in Channelrhodopsin-2. *Angew. Chem., Int. Ed. 54*, 4953.
(31) Furutani, Y., and Kandori, H. (2014) Hydrogen-bonding changes of internal water molecules upon the actions of microbial rhodopsins studied by FTIR spectroscopy. *Biochim. Biophys. Acta, Bioenerg. 1837*, 598−605.
(32) Kumar, S., Li, C., Montigny, C., le Maire, M., and Barth, A. (2013) Conformational changes of recombinant Ca2+-ATPase studied by reaction-induced infrared difference spectroscopy. *FEBS J. 280*, 5398−5407.
(33) Kötting, C., and Gerwert, K. (2015) What vibrations tell us about GTPases. *Biol. Chem. 396*, 131−144.
(34) Walker, J. W., Reid, G. P., McCray, J. A., and Trentham, D. R. (1988) Photolabile 1-(2-nitrophenyl)ethyl phosphate esters of adenine nucleotide analogs. Synthesis and mechanism of photolysis. *J. Am. Chem. Soc. 110*, 7170−7177.
(35) Melby, E. S., Soldat, D. J., and Barak, P. (2011) Synthesis and detection of oxygen-18 labeled phosphate. *PLoS One 6*, e18420.
(36) Park, C.-H., and Givens, R. S. (1997) New Photoactivated Protecting Groups. 6. *p* -Hydroxyphenacyl: A Phototrigger for Chemical and Biochemical Probes [1, 2]. *J. Am. Chem. Soc. 119*, 2453−2463.
(37) Goody, R. S. (1982) A simple and rapid method for the synthesis of nucleoside 5′-monophosphates enriched with 17O or 18O on the phosphate group. *Anal. Biochem. 119*, 322−324.
(38) Gavriljuk, K., Gazdag, E.-M., Itzen, A., Kötting, C., Goody, R. S., and Gerwert, K. (2012) Catalytic mechanism of a mammalian Rab·RabGAP complex in atomic detail. *Proc. Natl. Acad. Sci. U. S. A. 109*, 21348−21353.
(39) Taus, T., Köcher, T., Pichler, P., Paschke, C., Schmidt, A., Henrich, C., and Mechtler, K. (2011) Universal and confident phosphorylation site localization using phosphoRS. *J. Proteome Res. 10*, 5354−5362.
(40) Cepus, V., Scheidig, A. J., Goody, R. S., and Gerwert, K. (1998) Time-resolved FTIR studies of the GTPase reaction of H-ras p21 reveal a key role for the beta-phosphate. *Biochemistry 37*, 10263−10271.
(41) Gerwert, K., Souvignier, G., and Hess, B. (1990) Simultaneous monitoring of light-induced changes in protein side-group protonation, chromophore isomerization, and backbone motion of bacteriorhodopsin by time-resolved Fourier-transform infrared spectroscopy. *Proc. Natl. Acad. Sci. U. S. A. 87*, 9774−9778.
(42) Hessling, B., Souvignier, G., and Gerwert, K. (1993) A model-independent approach to assigning bacteriorhodopsin's intramolecular reactions to photocycle intermediates. *Biophys. J. 65*, 1929−1941.
(43) Goody, P. R., Heller, K., Oesterlin, L. K., Müller, M. P., Itzen, A., and Goody, R. S. (2012) Reversible phosphocholination of Rab proteins by Legionella pneumophila effector proteins. *EMBO J. 31*, 1774−1784.
(44) Michaely, P. (2002) Crystal structure of a 12 ANK repeat stack from human ankyrinR. *EMBO Journal 21*, 6387−6396.
(45) Kee, J.-M., and Muir, T. W. (2012) Chasing Phosphohistidine, an Elusive Sibling in the Phosphoamino Acid Family. *ACS Chem. Biol. 7*, 44−51.
(46) Givens, R. S., and Lee, J.-I. (2003) The p-Hydroxyphenacyl Photoremovable Protecting Group. *J. Photosci. 10*, 37−48.
(47) Corrie, J. E. T., Munasinghe, V. R. N., Trentham, D. R., and Barth, A. (2008) Studies of decarboxylation in photolysis of alpha-carboxy-2-nitrobenzyl (CNB) caged compounds. *Photochem. Photobiol. Sci. 7*, 84−97.
(48) Allin, C., Ahmadian, M. R., Wittinghofer, A., and Gerwert, K. (2001) Monitoring the GAP catalyzed H-Ras GTPase reaction at atomic resolution in real time. *Proc. Natl. Acad. Sci. U. S. A. 98*, 7754−7759.
(49) Gerwert, K., Hess, B., Soppa, J., and Oesterhelt, D. (1989) Role of aspartate-96 in proton translocation by bacteriorhodopsin. *Proc. Natl. Acad. Sci. U. S. A. 86*, 4943−4947.
(50) Schröter, G., Mann, D., Kötting, C., and Gerwert, K. (2015) Integration of Fourier Transform Infrared Spectroscopy, Fluorescence Spectroscopy, Steady-State Kinetics and Molecular Dynamics Simulations of $G\alpha_{i1}$ distinguishes between the GTP Hydrolysis and GDP Release Mechanism. *J. Biol. Chem. 290*, 17085−17095.
(51) Steitz, T. A., Smerdon, S. J., Jäger, J., and Joyce, C. M. (1994) A unified polymerase mechanism for nonhomologous DNA and RNA polymerases. *Science 266*, 2022−2025.
(52) Onidas, D., Stachnik, J. M., Brucker, S., Krätzig, S., and Gerwert, K. (2010) Histidine is involved in coupling proton uptake to electron transfer in photosynthetic proteins. *Eur. J. Cell Biol. 89*, 983−989.
(53) Müller, M. P., Albers, M. F., Itzen, A., and Hedberg, C. (2014) Exploring adenylylation and phosphocholination as post-translational modifications. *ChemBioChem 15*, 19−26.

DOI: 10.1021/acs.biochem.6b00524
Biochemistry 2016, 55, 4375−4385

Supporting Information

Unraveling the Phosphocholination Mechanism of the Legionella pneumophila Enzyme AnkX

Konstantin Gavriljuk,[†,‖] Jonas Schartner,[†] Hans Seidel,[†,‖] Clarissa Dickhut,[‡] Rene P. Zahedi,[‡] Christian Hedberg,[§] Carsten Kötting,[*,†] and Klaus Gerwert[*,†]

[†] Department of Biophysics, Ruhr-Universität Bochum, Universitätsstrasse 150, 44801 Bochum, Germany

[‡] Leibniz-Institut für Analytische Wissenschaften-ISAS-e.V., Otto-Hahn-Strasse 6b, 44227 Dortmund, Germany

[§] Department of Chemistry and Umea Center for Microbial Research, Umea University, SE-90187 Umea, Sweden

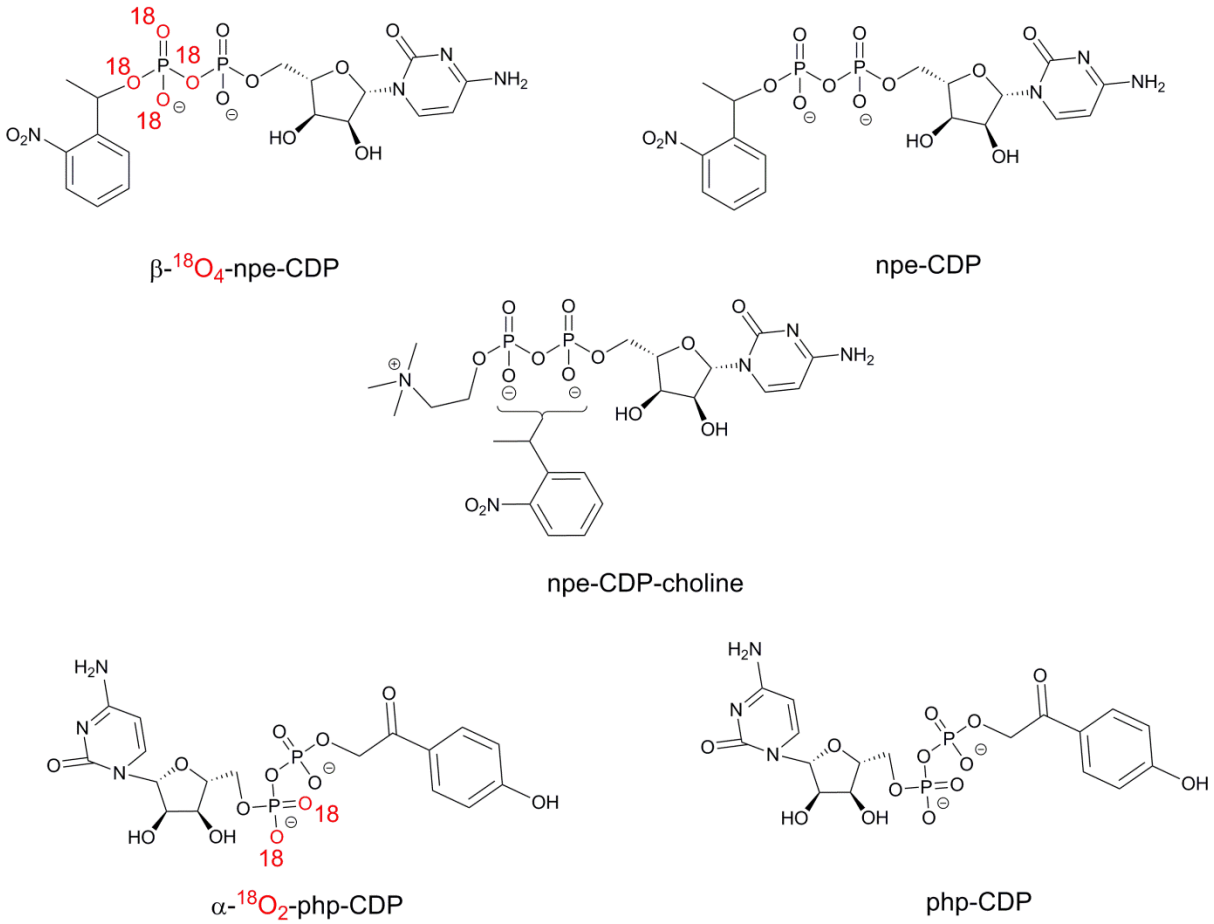

Supplementary Figure 1: Overview of the synthesized caged compounds.

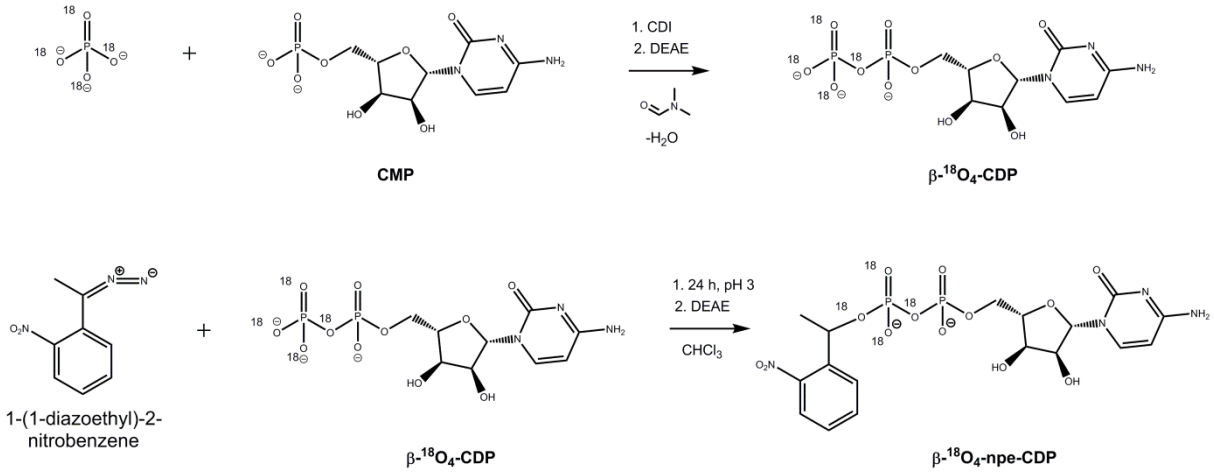

Supplementary Figure 2: Synthesis of β-$^{18}O_4$-npe-CDP. In the first step, ^{18}O-phosphate is coupled to CMP yielding in β-$^{18}O_4$-CDP. To β-$^{18}O_4$-CDP 1-(1-diazoethyl)-2-nitrobenzene is covalently attached, which results in the desired product β-$^{18}O_4$-npe-CDP.

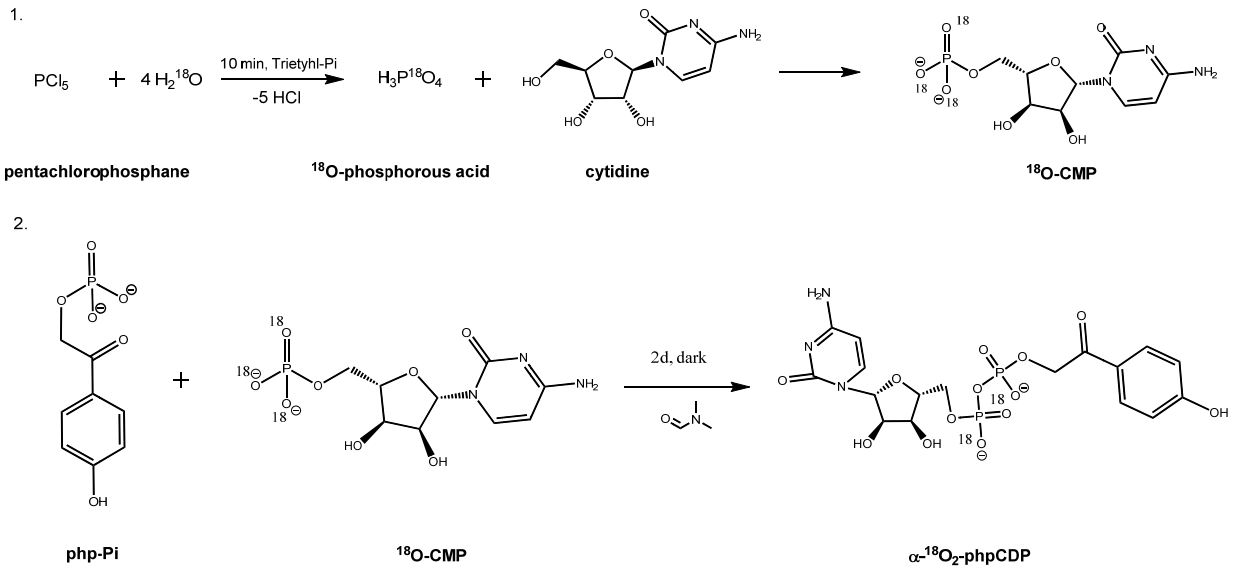

Supplementary Figure 3: Synthesis of α-$^{18}O_2$-php-CDP. The reaction of pentachlorophosphane with $H_2{}^{18}O$ yields in ^{18}O-phosphorous acid that is further reacted with cytidine, resulting in ^{18}O-labeled CMP. After the coupling of php-phosphate with ^{18}O-CMP, the desired product α-$^{18}O_2$-php-CDP was obtained.

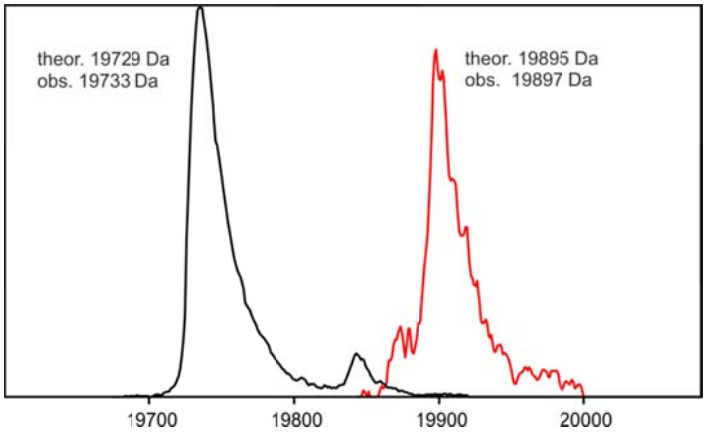

Supplementary Figure 4: ESI-MS spectra of a Rab1b$_{3-174}$ control sample (black) and an exemplary sample directly taken from the PCylation reaction with equimolar amounts of AnkX$_{1-652}$ (red). The spectra indicate a single PCylation of Rab1b. The red spectrum has a worse S/N ration due to the presence of equimolar AnkX ions in the measurement. Likewise, PCylation of Rab1b was observed with all investigated AnkX constructs.

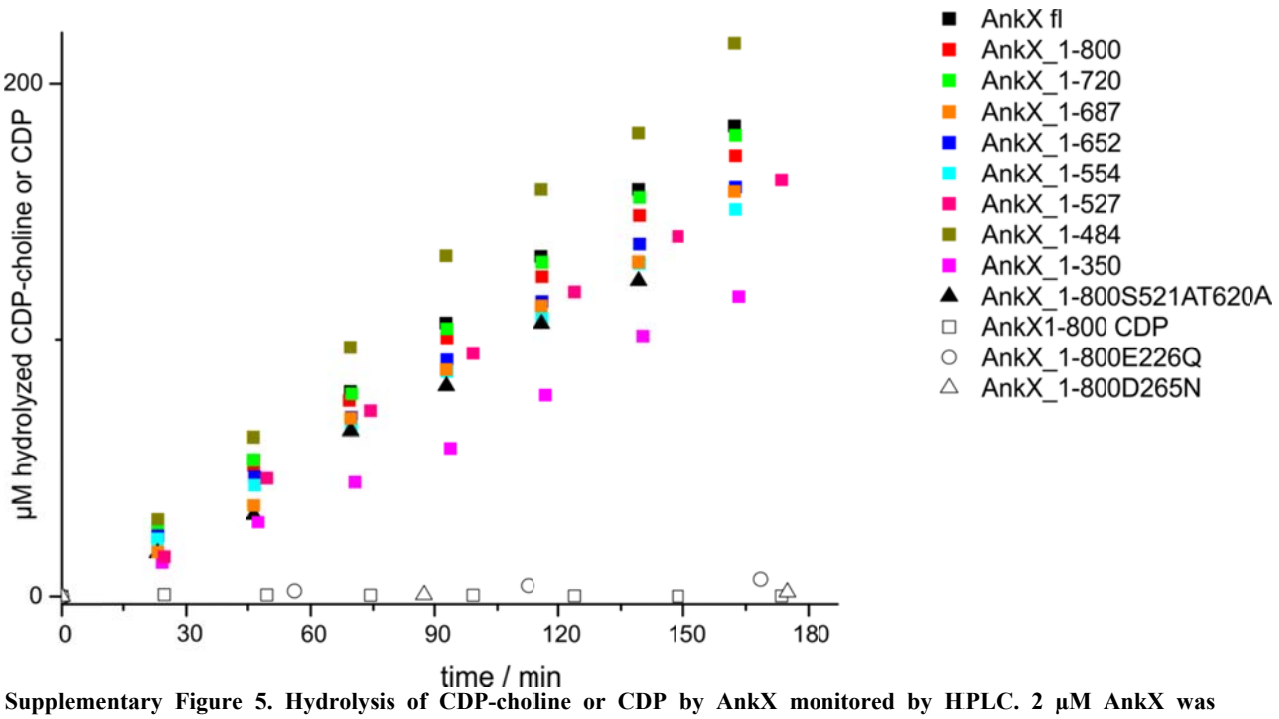

Supplementary Figure 5. Hydrolysis of CDP-choline or CDP by AnkX monitored by HPLC. 2 µM AnkX was incubated with 1 mM substrate at 25 °C. All AnkX constructs hydrolyze CDP-choline at a similar rate, while the mutants E226Q and D265N are inactive. CDP is not a substrate for hydrolysis.

Supplementary Table 1: ESI-MS analysis of AnkX autoPCylation. The data were taken from the same measurements that showed PCylation of Rab1b with all constructs, except when indicated that no Rab1b was included during incubation with CDP-choline. Control measurements without CDP-choline were performed separately but also included Rab1b for better comparability of the S/N ratio in the data. All constructs longer than 1-484 are PCylated. The experiment with AnkXH229A using catalytic amount of AnkX wild-type shows that the automodification occurs intramolecularly.

Construct	Theor. mass / Da	Exp. mass / Da	Theor. mass for double PCylation	Exp. mass for PCylation
full length	107085	107125	107417	107431
1-800 (12 ank repeats)	90449	90453	90781	90634/90786
1-720 (10 repeats)	81180	81183	81512	81511
1-687 (9 repeats)	no MS data			
1-652(8 repeats)	73615	73626	73947	73784/73954
1-554 (5 repeats)	62856	62861	63188	63020/63191
1-527 (4 repeats)	59751	59755	60083	60583
1-484 (2.5 repeats)	55105	55108	55437	55113
1-350 (no ank repeats)	40492	40499	40824	40504
1-800H229A catalyzed with 1% WT (no Rab1b)	90383	90410	90715	90388

Phosphocholine transferase AnkX, ankX, Q5ZXN6
Legionella pneumophila subsp. pneumophila
Sequence Coverage 53.1 %

S521
514IFDELLNsGADISDELLDAIWAR536
z=3, 914.45209 m/z, Δ -0.65 ppm
Mascot Score 52 (MD 18), ptmRS Score S8(Pc): 100 %

ETD fragment ion spectrum and ion table.
Δ = mass deviation from theoretical percursor mass
MD = Mascot Delta Score

#1	c'	c²⁺	Seq.	y'	y²⁺	z'	z²⁺	z+2'	z+2²	#2
1	131.11790	66.06259	I							23
2	278.18632	139.59680	F	2628.25942	1314.63335	2612.24070	1306.62399	2614.25635	1307.61181	22
3	393.21327	197.11027	D	2481.19100	1241.09914	2465.17228	1233.08978	2467.18793	1234.09760	21
4	522.25587	261.63157	E	2366.16405	1183.58566	2350.14533	1175.57630	2352.16098	1176.54413	20
5	635.33994	318.17361	L	2237.12145	1119.06436	2221.10273	1111.05500	2223.11838	1112.06283	19
6	748.42401	374.71564	L	2124.03738	1062.52233	2108.01866	1054.51297	2110.03431	1055.52079	18
7	862.46694	431.73711	N	2010.95331	1005.98029	1994.93459	997.97093	1996.95024	998.97876	17
8	1114.55445	557.78086	S-Pc	1896.91038	948.95883	1880.89166	940.94947	1882.90731	941.95729	16
9	1171.57592	586.29160	G	1644.82287	822.91507	1628.80415	814.90571	1630.81980	815.91354	15
10	1242.61304	621.81016	A	1587.80140	794.40434	1571.78268	786.39498	1573.79833	787.40280	14
11	1357.63999	679.32363	D	1516.76428	758.88578	1500.74556	750.87642	1502.76121	751.88424	13
12	1470.72406	735.86567	I	1401.73733	701.37230	1385.71861	693.36294	1387.73426	694.37077	12
13	1557.75609	779.38168	S	1288.65326	644.83027	1272.63454	636.82091	1274.65019	637.82873	11
14	1672.78304	836.89516	D	1201.62123	601.31425	1185.60251	593.30489	1187.61816	594.31272	10
15	1801.82564	901.41646	E	1086.59428	543.80078	1070.57556	535.79142	1072.59121	536.79924	9
16	1914.90971	957.95849	L	957.55168	479.27948	941.53296	471.27012	943.54861	472.27794	8
17	2027.99378	1014.50053	L	844.46761	422.73744	828.44889	414.72808	830.46454	415.73591	7
18	2143.02073	1072.01400	D	731.38354	366.19541	715.36482	358.18605	717.38047	359.19387	6
19	2214.05785	1107.53256	A	616.35659	308.68193	600.33787	300.67257	602.35352	301.68040	5
20	2327.14192	1164.07460	I	545.31947	273.16337	529.30075	265.15401	531.31640	266.16184	4
21	2513.22124	1257.11426	W	432.23540	216.62134	416.21668	208.61198	418.23233	209.61980	3
22	2584.25836	1292.63282	A	246.15608	123.58168	230.13736	115.57232	232.15301	116.58014	2
23			R	175.11896	88.06312	159.10024	80.05376	161.11589	81.06158	1

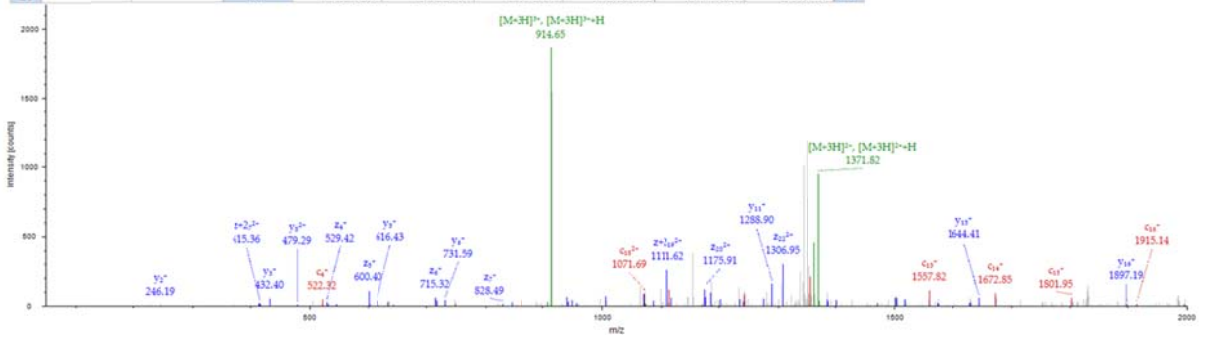

T620

^{617}LTDtSGNSVLHYVFYSK^{633}

z=3, 699.34058 m/z, Δ -1.37 ppm

Mascot Score 81(MD 13), ptmRS Score T4(Pc): 100 %

ETD fragment ion spectrum and ion table.
Δ = mass deviation from thereotical percursor mass
MD = Mascot Delta Score

#1	c⁺	c²⁺	Seq.	y⁺	y²⁺	z⁺	z²⁺	z+2⁺	z+2²⁺	#2
1	131.11790	66.06259	L							17
2	232.16558	116.58643	T	1982.92597	991.96662	1966.90725	983.95726	1968.92290	984.96509	16
3	347.19253	174.09990	D	1881.87829	941.44278	1865.85957	933.43342	1867.87522	934.44125	15
4	613.29569	307.15148	T-Pc	1766.85134	883.92931	1750.83262	875.91995	1752.84827	876.92777	14
5	700.32772	350.66750	S	1500.74818	750.87773	1484.72946	742.86837	1486.74511	743.87619	13
6	757.34919	379.17823	G	1413.71615	707.36171	1397.69743	699.35235	1399.71308	700.36018	12
7	871.39212	436.19970	N	1356.69468	678.85098	1340.67596	670.84162	1342.69161	671.84944	11
8	958.42415	479.71571	S	1242.65175	621.82951	1226.63303	613.82015	1228.64868	614.82798	10
9	1057.49257	529.24992	V	1155.61972	578.31350	1139.60100	570.30414	1141.61665	571.31196	9
10	1170.57664	585.79196	L	1056.55130	528.77929	1040.53258	520.76993	1042.54823	521.77775	8
11	1307.63555	654.32141	H	943.46723	472.23725	927.44851	464.22789	929.46416	465.23572	7
12	1470.69887	735.85307	Y	806.40832	403.70780	790.38960	395.69844	792.40525	396.70626	6
13	1569.76729	785.38728	V	643.34500	322.17614	627.32628	314.16678	629.34193	315.17460	5
14	1716.83571	858.92149	F	544.27658	272.64193	528.25786	264.63257	530.27351	265.64039	4
15	1879.89903	940.45315	Y	397.20816	199.10772	381.18944	191.09836	383.20509	192.10618	3
16	1966.93106	983.96917	S	234.14484	117.57606	218.12612	109.56670	220.14177	110.57452	2
17			K	147.11281	74.06004	131.09409	66.05068	133.10974	67.05851	1

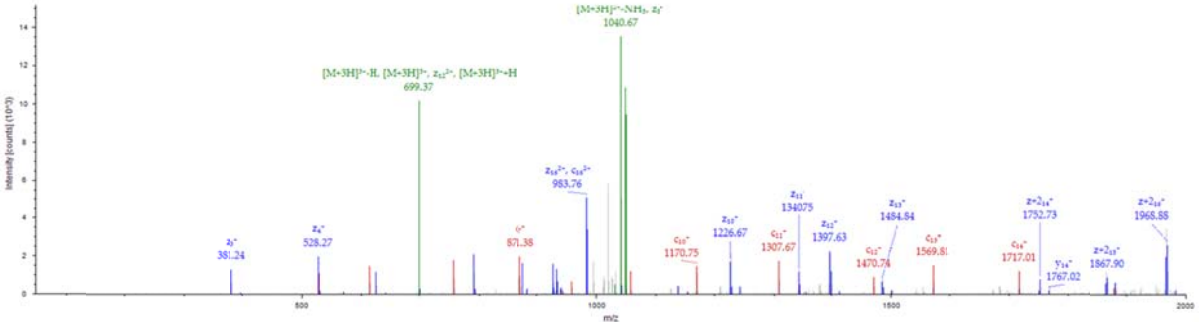

T943

^{936}SIQEAVGtSLK^{946}

z=3, 433.22986 m/z, Δ -1.03 ppm,

Mascot Score 67 (MD 17), ptmRS Score T8(Pc): 99.99 %

ETD fragment ion spectrum and ion table.
Δ = mass deviation from thereotical percursor mass
MD = Mascot Delta Score

#1	c⁺	c²⁺	Seq.	y⁺	y²⁺	z⁺	z²⁺	z+2⁺	z+2²⁺	#2
1	105.06586	53.03657	S							11
2	218.14993	109.57860	I	1210.64433	605.82580	1194.62561	597.81644	1196.64126	598.82427	10
3	346.20851	173.60789	Q	1097.56026	549.28377	1081.54154	541.27441	1083.55719	542.28223	9
4	475.25111	238.12919	E	969.50168	485.25448	953.48296	477.24512	955.49861	478.25294	8
5	546.28823	273.64775	A	840.45908	420.73318	824.44036	412.72382	826.45601	413.73164	7
6	645.35665	323.18196	V	769.42196	385.21462	753.40324	377.20526	755.41889	378.21308	6
7	702.37812	351.69270	G	670.35354	335.68041	654.33482	327.67105	656.35047	328.67887	5
8	968.48128	484.74428	T-Pc	613.33207	307.16967	597.31335	299.16031	599.32900	300.16814	4
9	1055.51331	528.26029	S	347.22891	174.11809	331.21019	166.10873	333.22584	167.11656	3
10	1168.59738	584.80233	L	260.19688	130.60208	244.17816	122.59272	246.19381	123.60054	2
11			K	147.11281	74.06004	131.09409	66.05068	133.10974	67.05851	1

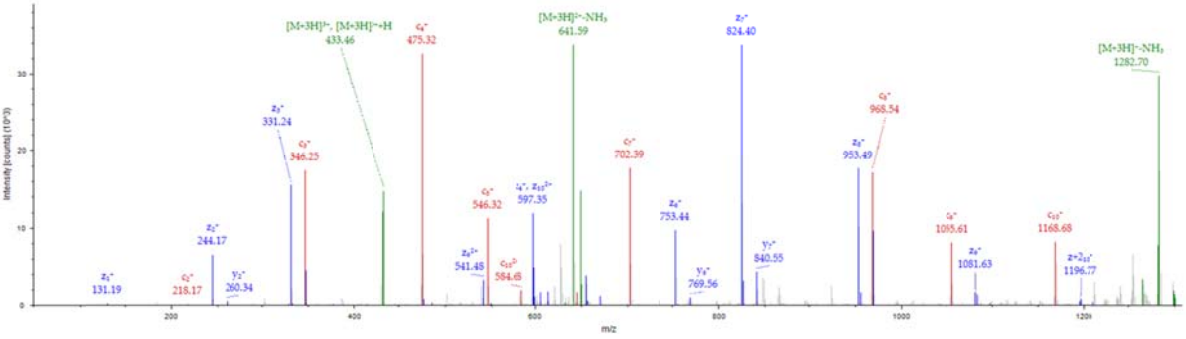

Supplementary Figure 6. Shotgun nano LC-MS data for the identification of autophosphocholination sites in AnkX.

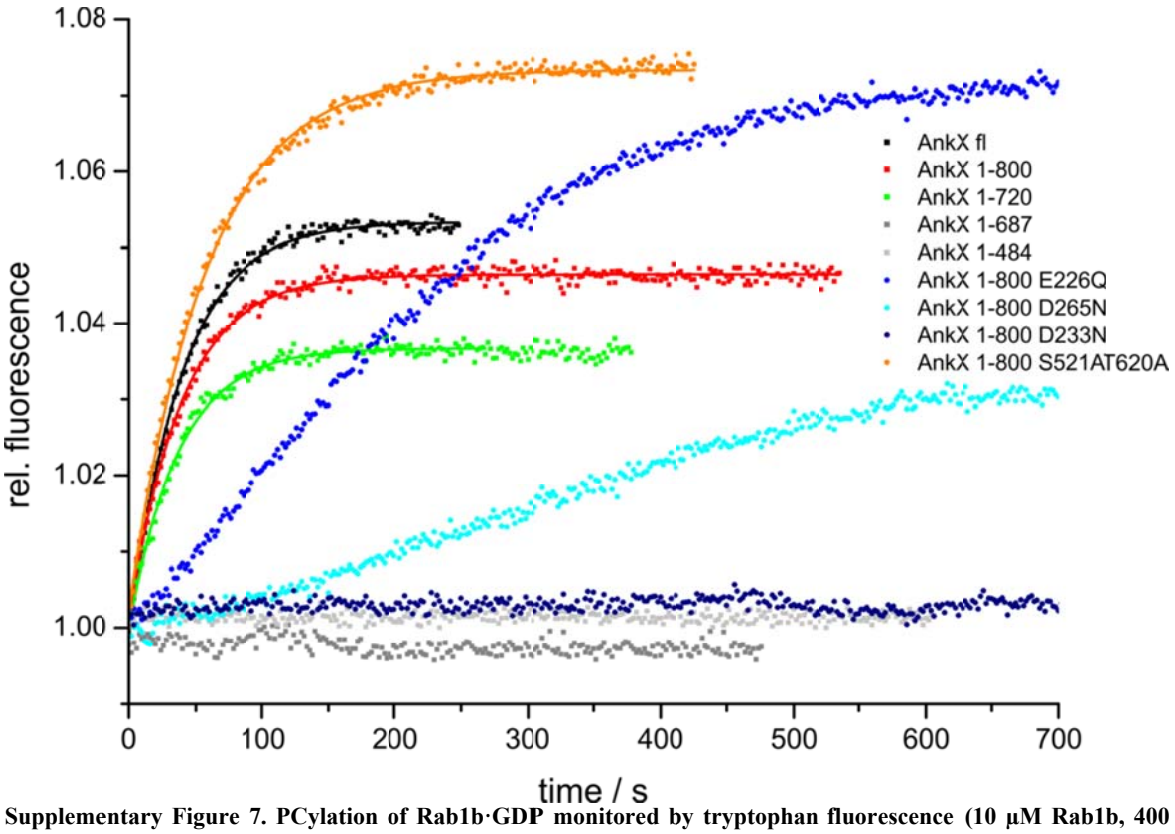

Supplementary Figure 7. PCylation of Rab1b·GDP monitored by tryptophan fluorescence (10 µM Rab1b, 400 µM CDP-choline, 200 nM AnkX at 25 °C). Lifetimes from monoexponential fits are: AnkX fl (39 ± 0.5 s), $AnkX_{1-800}$ (35 ± 0.4 s), $AnkX_{1-720}$ (37 ± 0.7 s), $AnkX_{1-800}$ S521AT620A (57 ± 0.5 s). The autoPCylation deficient mutant S521AT620A behaves similarly to the wild-type. AnkX D233N is inactive, while D265N retains little activity, and E226Q has strongly diminished activity (234 ± 3 s).

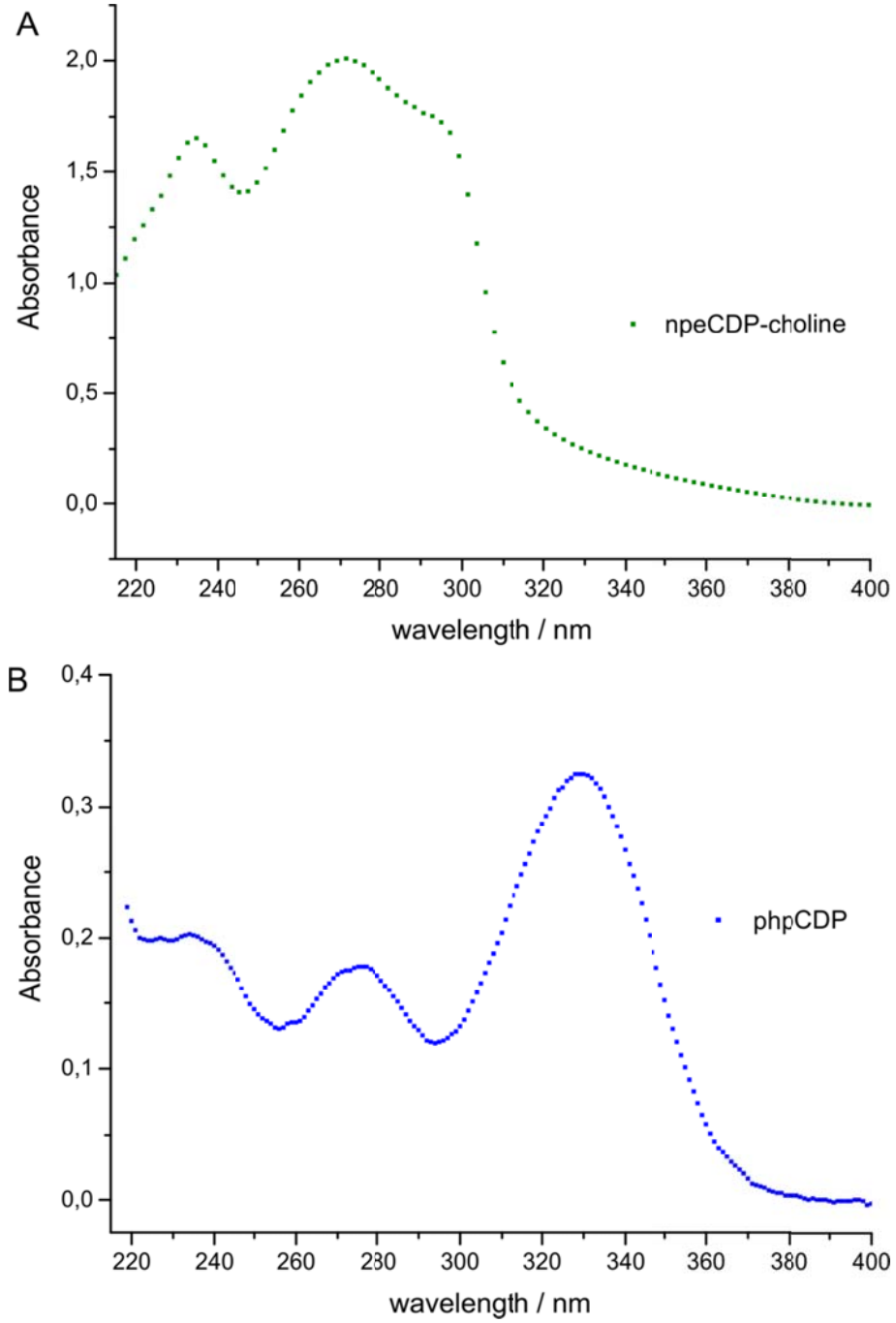

Supplementary Figure 8. Absorbance spectra of the caged compounds npeCDP-choline (A) and phpCDP (B).

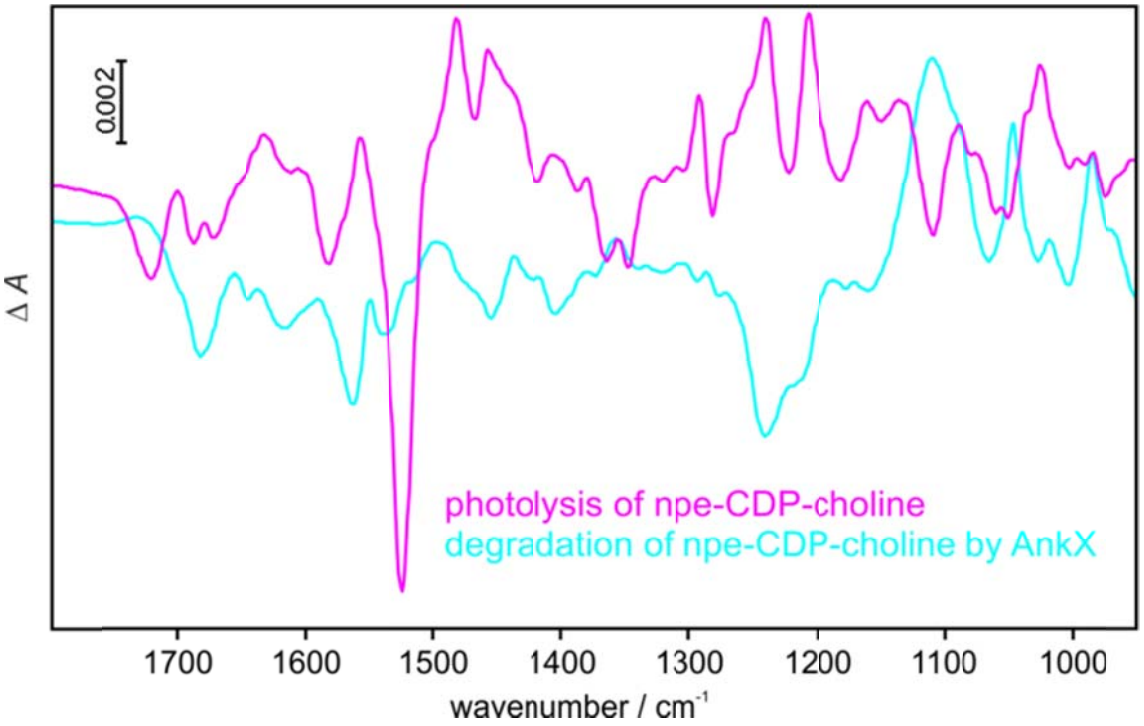

Supplementary Figure 9. Photolysis and degradation of npeCDP-choline. Synthesized npeCDP-choline could be photolyzed (magenta spectrum), but AnkX constantly degraded npeCDP-choline already prior to photolysis as shown by the cyan spectrum. While bands were not isotopically assigned, CMP seems to appear after degradation at 979 cm^{-1}. Also, no further reaction or difference bands in the photolysis could be obtained in the presence of Rab1b, which is consistent with the degradation of the caged compound.

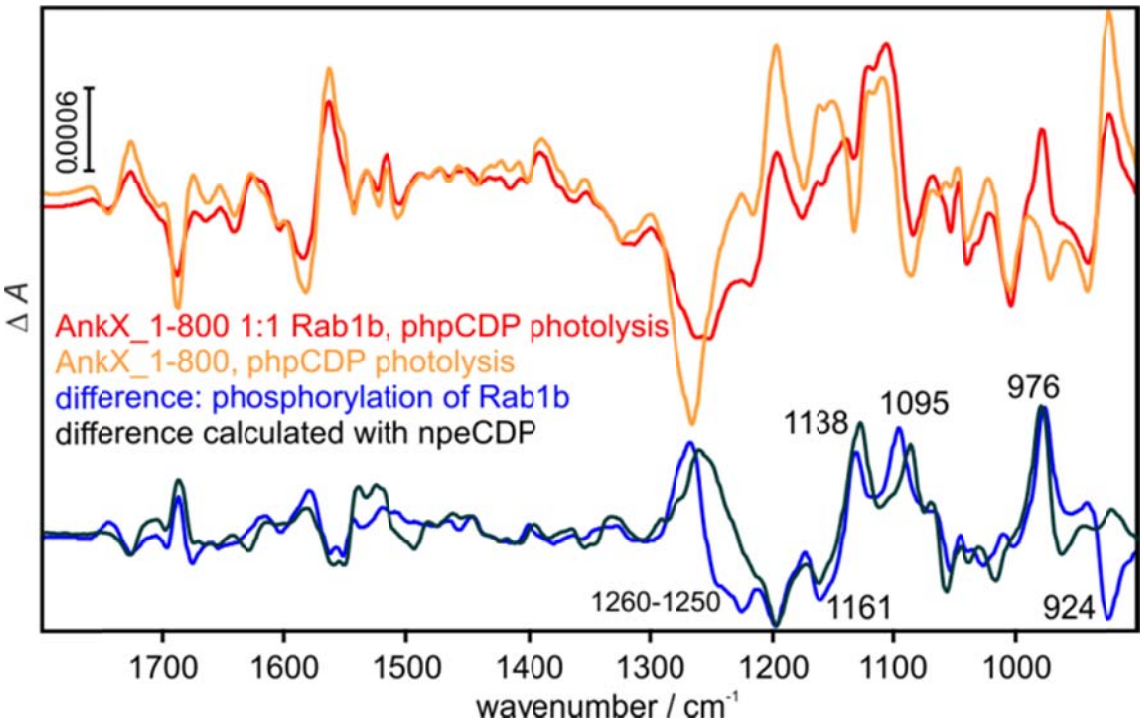

Supplementary Figure 10. Calculation of the difference spectrum of the Rab1b phosphorylation by AnkX. Since the phosphorylation reaction could not be kinetically resolved, we calculated the difference spectrum of the reaction (blue) from the photolysis spectra of AnkX + phpCDP without and with Rab1b (orange and red, respectively). This approach has some uncertainties, as demonstrated by the calculation using photolysis of npeCDP (result in black) instead of phpCDP because some bands belonging to the caged compounds cannot be subtracted completely (i.e. 924 cm^{-1} or 1260 – 1250 cm^{-1}). However, most of the bands can be reliably reproduced.

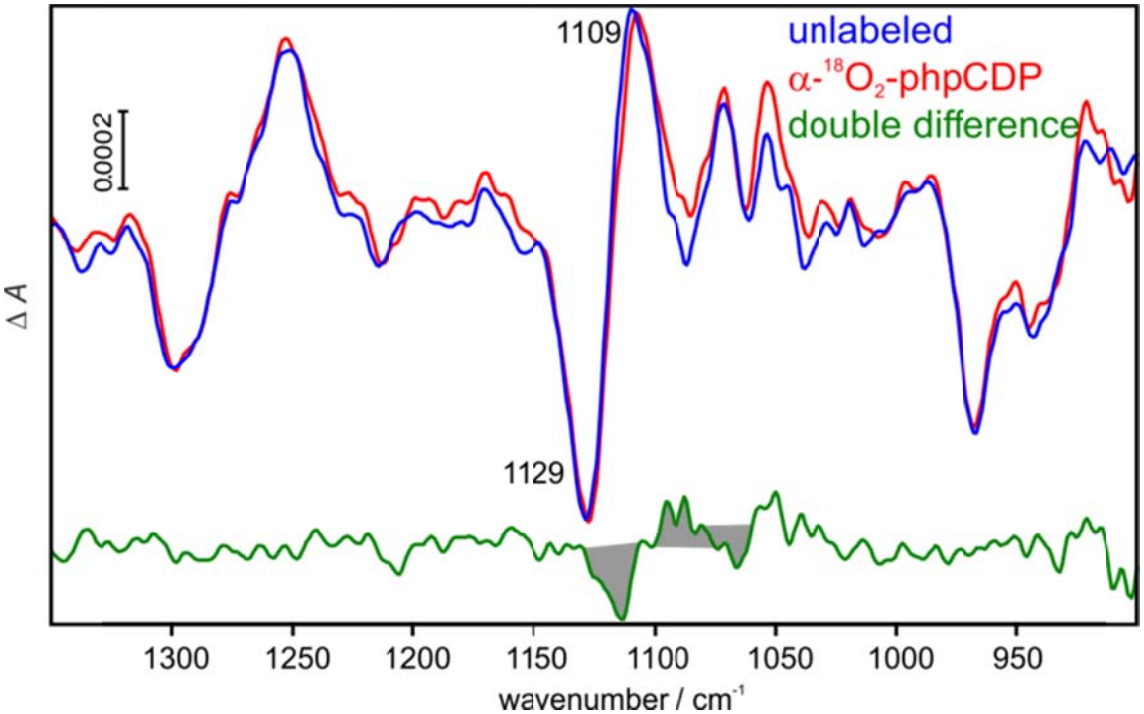

Supplementary Figure 11. Assignment of the α-phosphate bands in the infrared spectra of the precatalytic conformational change of AnkX using unlabeled (blue) and α-$^{18}O_2$-labeled phpCDP (red). Negative bands belong to the state with caged CDP, positive bands belong to the precatalytic state. The double difference (labeled - unlabeled) is shown in green. Small shifts are detected in the region of the negative band at 1129 cm^{-1} and the positive band at 1109 cm^{-1}. The bands most likely reflect a combination vibration of the two phosphates of CDP, but the contribution of the α-phosphate appears to be small and β-labeled phpCDP was not available. Therefore, it can be concluded that the conformational change does not strongly influence the α-phosphate. Also, it is clear that CDP is still present in this state because no CMP band is detected, which would appear at 979 cm^{-1}.

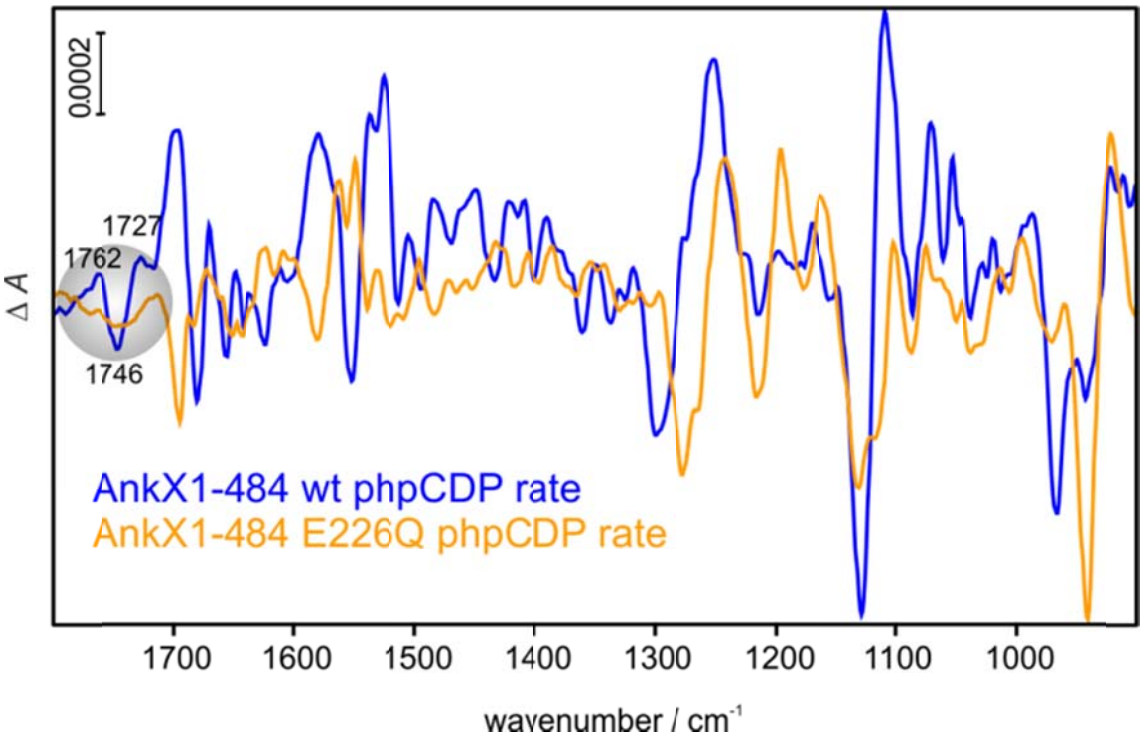

Supplementary Figure 12. Comparison of the amplitude spectra of the precatalytic conformational change in wild-type AnkX (blue) and AnkX E226Q (orange). Negative bands belong to the state directly after photolysis of caged CDP, positive bands belong to the precatalytic state. The bands in the phosphate region are similar to wild-type, although not the same. Importantly, the pattern in the carboxylic acid region (1762 – 1727 cm^{-1}) vanishes. This indicates that E226 is involved in the protonation change of the active site. The introduced amide group of the glutamine may be responsible for the negative band at 1693 cm^{-1}. The ten times slower kinetics of the conformational change indicate that the proton takes an alternative pathway. Overall, E226Q has a slightly different conformation as indicated by the altered spectrum, being consistent with its lower phosphocholinetransferase activity.

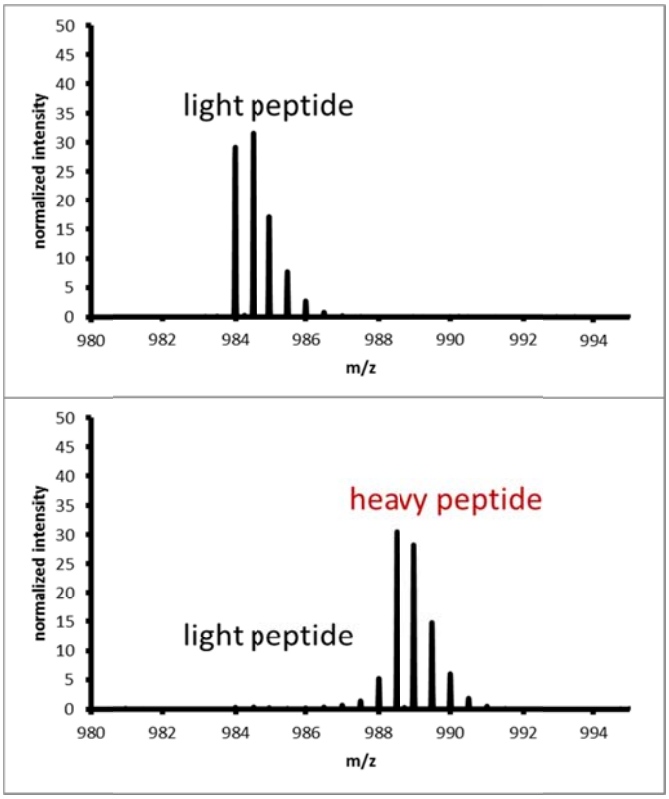

Supplementary Figure 13. MS/MS spectra of an AnkX$_{1-484}$ peptide (TPITLYGYhSSLEEQTK) show a 9 Da/z mass shift , confirming the successful incorporation of $^{13}C_6{}^{15}N_3$-His in the protein (efficiency > 98 %). Figure courtesy of Dr. C. Lindemann.

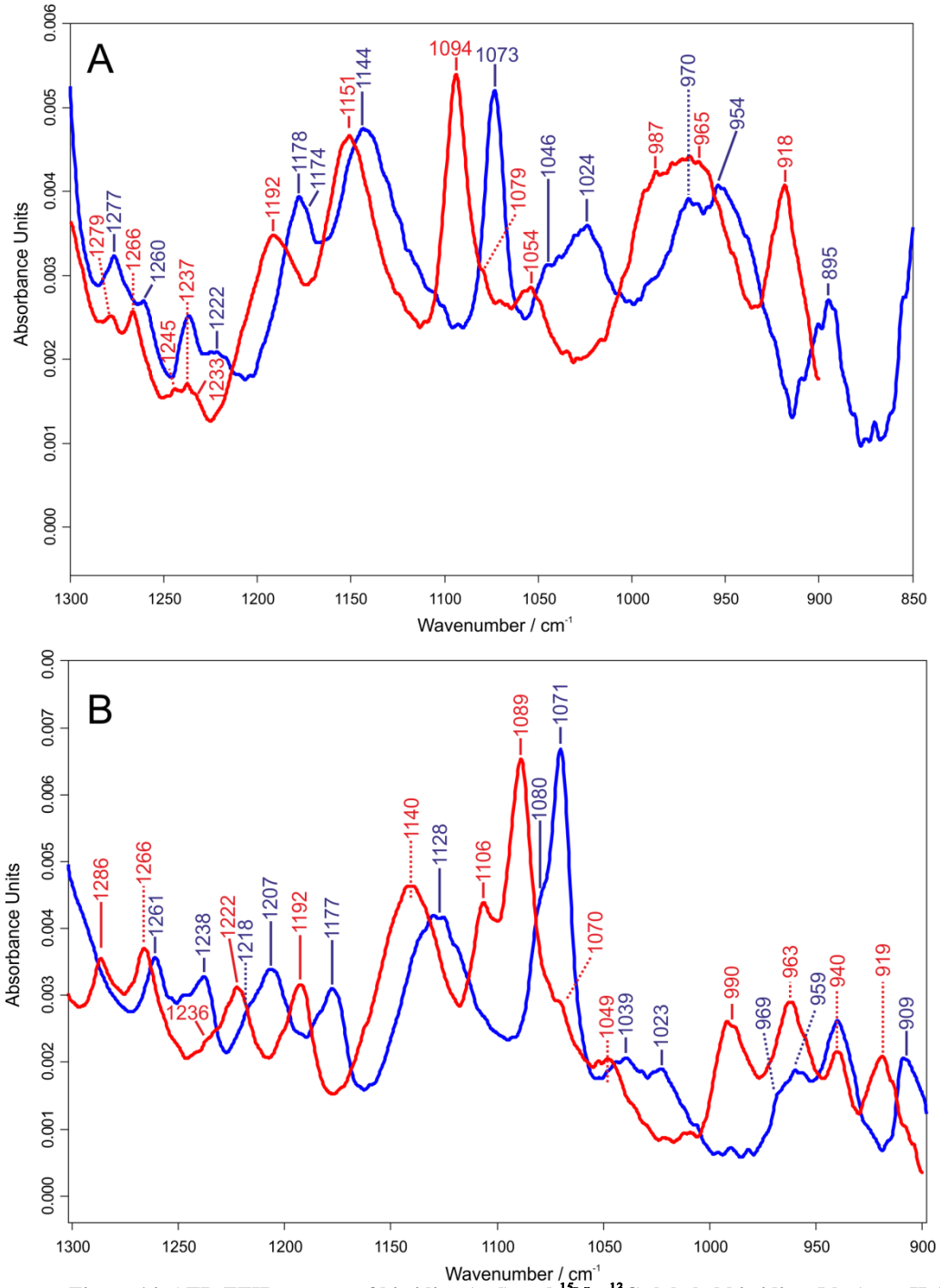

Supplementary Figure 14. ATR-FTIR spectra of histidine (red) and $^{15}N_3$–$^{13}C_6$-labeled histidine (blue) at pH 4 (A) and 7.7 (B). The imidazole group is protonated and positively charged at pH 4, while it is uncharged at pH 7.7. For example, this results in lower absorbance at 1192 and 1151 cm^{-1}, and thus in negative bands in the difference spectrum of the precatalytic conformational change. With isotopic labeling, the bands appear positive in the double difference labeled-unlabeled, as seen in Figure 6. In another example, the band at 1106 cm^{-1} appears in the deprotonated state, so it would be positive in the difference spectrum of the reaction and negative in the double difference. Data of the isolated compounds and this figure are courtesy of Dr. D. Onidas.